Scientific Research Publishing

Computational Chemistry, 2025, 13(4), 102-133
https://www.scirp.org/journal/cc
ISSN Online: 2332-5984
ISSN Print: 2332-5968

Computational Studies on Keto-Enol Tautomerism of Mesoxaldehyde, 1,2-Bis-Phenyl Hydrazone (MBPH) in the Gas Phase Using HF and DFT Methods, to Investigate the Possibility of Using This Structure for the Synthesis of Different Heterocyclic Compounds, Confirmed by Spectral Tools

Sohila H. Mancy[1], Mohamed A. El Sekily[2], Nagwa M. M. Hamada[1*]

[1]Department of Physics and Chemistry, Faculty of Education, University of Alexandria, Alexandria, Egypt
[2]Department of Chemistry, Faculty of Science, University of Alexandria, Alexandria, Egypt
Email: *nagwahamada2002@alexu.edu.eg, *nagwahamada2002@g mail.com

How to cite this paper: Mancy, S.H., El Sekily, M.A. and Hamada, N.M.M. (2025) Computational Studies on Keto-Enol Tautomerism of Mesoxaldehyde, 1,2-Bis-Phenyl Hydrazone (MBPH) in the Gas Phase Using HF and DFT Methods, to Investigate the Possibility of Using This Structure for the Synthesis of Different Heterocyclic Compounds, Confirmed by Spectral Tools. *Computational Chemistry*, **13**, 102-133.
https://doi.org/10.4236/cc.2025.134005

Received: July 15, 2025
Accepted: September 5, 2025
Published: September 8, 2025

Abstract

In this article, the optimized geometries of six possible tautomers of mesoxaldehyde 2,3-bis-phenyl hydrazone (MBPH) **(1)** have been studied in the gas phase by ab initio Hartree-Fock (HF) and density Functional theories DFT with different levels of theory, B3LYP, B3PW91, WB97XD, with 6-311G(d,p) basis set. The different conformers of the compound were studied using the B3LYP functional with a 6-311G(d,p) basis set. Optimum molecular geometries, electronic properties, and energetics of these systems have been discussed as the energy gap was determined using HOMO and LUMO energy values. Also, the reactivity descriptors such as Hardness (η), Softness ($1/\eta$), electronegativity index (χ), Chemical potential (μ), Electrophilicity ($\omega = \mu 2/2\eta$), and Nucleophilicity ($E_{HOMO} + 9.12$), indicate the electrophilic and nucleophilic nature of the different tautomers. The most stable conformer with the minimum energy was identified. This conformer was used for further computations, and electrophilic and nucleophilic regions have been identified with the aid of an MESP plot. The contour map shows electron density flow in the molecule. Thermodynamic properties and tautomeric equilibria between different tautomers were calculated using frequency calculations. Finally, mesoxaldehyde is used as a starting material to synthesize new heterocycles identified by different spectral tools.

Keywords

Mesoxaldehyde, HOMO, Hatree-Fock, MESP, B3LYP, B3PW91, WB97XD

1. Introduction

Quantum chemistry calculations are a rapid and inexpensive alternative to experimental techniques for obtaining many properties. They are widely used both as predictive tools and to confirm or explain experimental results [1]-[3]. However, Computational chemistry is today's most rapidly expanding and exciting area of scientific research. Quantum chemical ab initio programs have been used by the principles of quantum mechanics to obtain properties of molecular geometries, vibrational frequencies, barriers to rotation, ionization potentials, electron affinities, and many other properties [4]. Hartree-Fock theory, developed by D.R. Hartree [5] and V. Fock [6], is an ab initio method used to obtain approximate solutions of quantum many-body systems. Since the instantaneous Coulomb electron-electron repulsion is not considered, HF is the simplest type of ab initio electronic structure calculation. The approximate energies of a system obtained by HF theory are always equal to or larger than the exact energy [7]. However, due to electron exchange and correlation effects being ignored, the computational cost or time is low for HF method. In many types of computations, HF is usually the first calculation performed. Then, the results are corrected by applying methods that include the effects of electron-electron repulsion [7] [8]. DFT is one such method that includes electron exchange and correlation. Density functional theory (DFT), which was started by P. Hohenberg and W. Kohn in 1964 [9], is a theory in which electronic ground state energy is based on the electron density distribution n (r). [10]. It suffices to know the average number of electrons located at any one point in space, or the density of electrons, which largely reduces the degree of freedom and makes the computation much simpler. This simplicity makes it possible to study very large molecular systems. By including some of the effects of electron correlation, DFT methods have much more accuracy than HF theory at a modest increase in computational cost. [11]. Various functionals have been defined by exchange and correlation components i.e., local exchange and correlation functionals, and gradient-corrected functionals. Gradient-corrected exchange functional B proposed by Becke in 1988 [12] and the widely used gradient-corrected correlation functional LYP developed by Lee, Yang, and Parr [13] [14] form the famous B-LYP method. The DFT method used in the present study is B3LYP functional, which denotes Becke, three-parameter hybrid, Lee-Yang-Parr exchange-correlation functional. It is important to calculate the number of basis functions used to describe a molecule, as it proves useful for estimating the computational time. Splitting the valence is the first way to accomplish an increase in the size of the basis set; it is done by increasing the number of basis functions per atom. For example, 6-311G is a triple split valence basis, in which the core orbitals

are a contraction of six Gaussian type functions, and the valence split into three functions, represented by a contraction of three, one, and one, Gaussian type functions, respectively [15]. In the present work we have investigated theoretically the optimized geometries, vibrational spectra, thermodynamic properties, dipole movements and global descriptors of mesoxaldehyde tautomers, as a carbonyl compound by performing HF and DFT calculations. The reaction patterns of the specific classes of carbonyl compounds are related by the importance of tetrahedral intermediates, and differences in reactivity can often be traced to structural features present in those intermediates. In broad terms, there are three possible mechanisms for the addition of a nucleophile and a proton to give a tetrahedral intermediate in a carbonyl addition reaction [16].

a) Protonation followed by nucleophilic attack on the protonated carbonyl group:

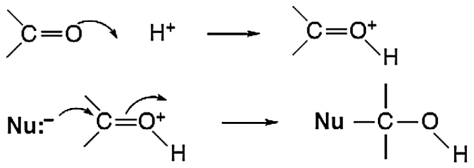

b) Nucleophilic addition at the carbonyl group followed by protonation:

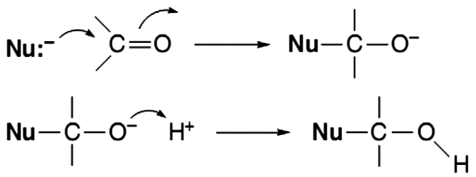

c) Concerted proton transfer and nucleophilic attack:

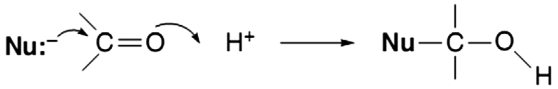

The nucleophile is shown as an anion, but can also be a neutral species, in which case a proton is subsequently lost. Additionally, it is well known that aliphatic carbonyl compounds, which have alpha hydrogens attached to the carbonyl group, undergo keto-enol tautomerism (**Figure 1**).

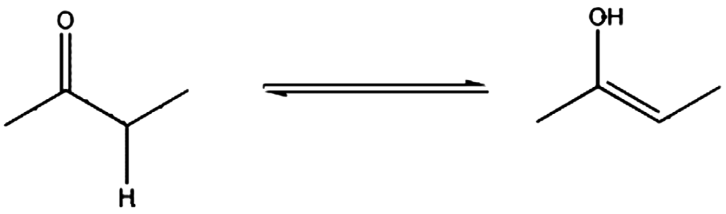

Figure 1. Keto-enol tautomerism.

It has been reported that **mesoxaldehyde 1,2-bis phenylhydrazone (1)** was obtained from sugar phenyl osazones on oxidation with periodic acid. It was interesting to study the type of chelation in **(1)**.

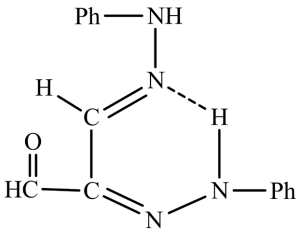

(1)

Since the imino proton of the phenyl hydrazone residue on C-2 could form a chelated ring [17], this attracts our attention to the computational study of the keto-enol tautomerism of **mesoxaldehyde-1,2-bis phenyl hydrazone (1),** and also uses it as a starting compound to obtain some different heterocycles, which can be identified with different spectral tools.

In an intramolecular hydrogen bond (IHB) system, both proton donor and proton acceptor groups, which may be of various kinds of functional groups, are located in the same molecule. The interaction of these functional groups may result in a ring-like structure that is often referred to as a chelated ring. The cis-enol forms of β-diketone, β-aminoenone, and β-enaminoimine molecules are engaged in such a hydrogen bond system and could be stabilized by a six-membered chelated ring [18]-[20]. Formation of IHB in these systems leads to an enhancement of resonance conjugation in the π-electron system. This kind of hydrogen bond was named by Gilli *et al.* [21] as a resonance-assisted hydrogen bond (RAHB). Formation of this kind of hydrogen bond causes an obvious affinity for bond equalization of the valence bonds in the resulting chelated ring.

2. Computational Methods

The *ab initio* and density functional theory methods were used to optimize the geometry of the six tautomers of mesoxaldehyde. The optimization processing was carried out with the aid of the Gaussian 09 W package [22]. Hartree Fock (HF) of ab initio methods [23] and Becke's three parameters exact exchange functional (B3) [24] combined with gradient corrected correlation functional of Lee-Yang-Parr (LYP) [25], Perdew and Wang's 1991 (PW91) [26] and the range separated hybrid WB97XD [27] of DFT method were employed to optimize the tautomers by using the 6-311G* basis set.. All calculations are performed on a Pentium IV/3.02 GHz personal computer. No imaginary frequency has been recorded during the optimization process, and we have not applied any constraints. Gauss View 5.0 and Chemcraft programs [28] [29] have been used to extract the computation results and to visualize the optimization structures as well as to draw the frontier molecular orbital (FMOs), molecular electrostatic potential (MEP) maps [30]. The electronic absorption spectra for the optimized molecule were calculated

with the time-dependent SCF (TD-SCF) theory at the B3LYP/6-311G(d,p) level in chloroform and ethanol. The harmonic vibrational frequencies were calculated using the analytical second derivatives at the HF/6-311G and B3LYP/6-311G level of theory. The thermodynamic functions, such as the heat capacity, entropy, and enthalpy, were calculated from the vibrational frequencies calculated using the same method and basis set. Several structural parameters are selected from the results of quantum computation such as Mulliken electron population, highest occupied molecular orbital energy (E_{HOMO}), lowest unoccupied molecular orbital energy (E_{LUMO}), and energy gap (E_{gap}), For further investigation, excellent tools to describe the reactivity and stability of compounds [31]-[33] included selective parameters such as ionization energy (IP), and electron affinity electrophilicity index (ω). These parameters are used to analyze reactivity [34] at the electrophilic sites in the compound **(1)**.

3. Results and Discussion

The phenomenon of keto-enol equilibrium is called "Tautomerism", and the forms are known as tautomers. The keto-enol equilibrium depends on the electronic features of the substituents, temperature, and the environment of the solvent. Under usual conditions, when one tautomer is more stable than the others, it is known as the "stable form". An intramolecular hydrogen bond is present in closed cis-enol forms, and it leads to a stable form of the tautomer [35] [36]. Herein, we discuss the behavior of different tautomers of the title compound computationally and chemically by preparing different heterocyclic compounds using it as a starting material (**Figure 2**).

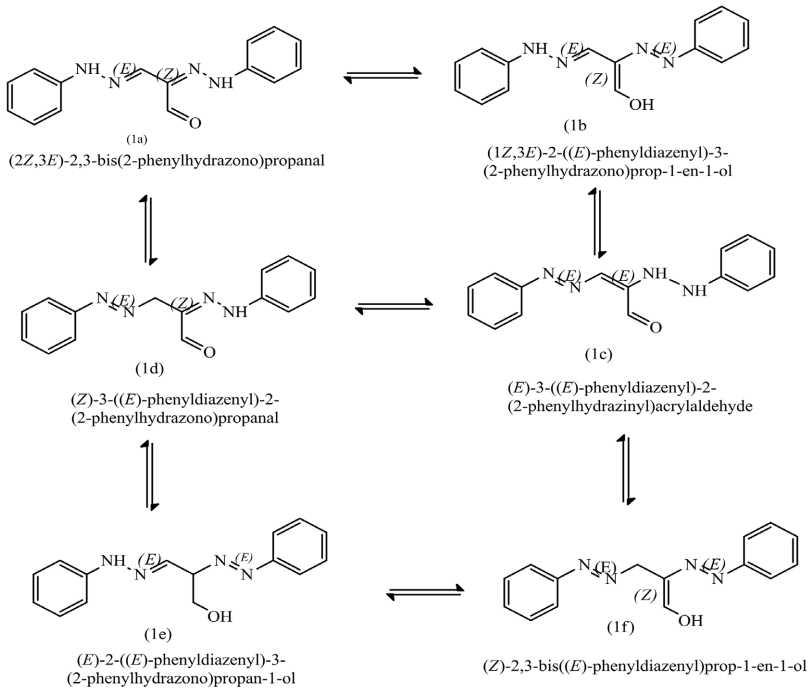

Figure 2. Different tautomers of mesoxaldehyde 1,2-bis-phenyl hydrazone (MBPH).

3.1. Computational Studies

I. Optimization calculations

The tautomerism of organic compounds has been the subject of extensive theoretical studies by using different quantum chemical methods [37]. The present work aimed to characterize the tautomerization of the molecular structure, reactivity descriptors, frequencies, and chemical shifts of the six tautomers of MBPH. Hartree-Fock and Density Functional Theory computational codes are used in practice to investigate the structural, magnetic, and electronic properties of all tautomers. The stability and chemical reactivity of these tautomers in the gas phase have been predicted by using the well-known quantum-chemical methods described above. However, DFT calculations produce the electron densities of molecules with good results. The title compound was computed using HF/6-311G(d,p), DFT/B3LYP, 6-311G(d,p), DFT/B3PW91, 6-311G(d,p) and DFT/WB97XD, 6-311G(d,p) in the gas phase, this set was chosen to compare results from a standard hybrid functional with a range-separated one would strengthen the methodology. The optimized structure of the computed tautomer calculated at B3LYP/6-311G(d,p) is shown in Figure 3.

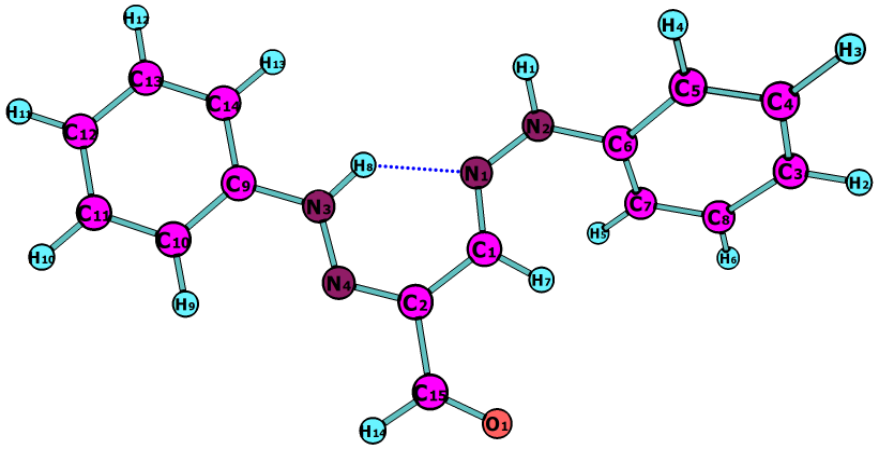

Figure 3. Optimized molecular structure of MBPH calculated at DFT/B3LYP/6-311G(d,p) with atom numbering scheme *via* the Chemcraft program.

II. Structural Analysis

A detailed analysis of the structural and energetical changes caused by the migration of hydrogen atoms would enable us to understand the different properties of the tautomers. Most of the tautomers were not studied by experiment due to their low concentration and stability. Quantum chemical calculations are the best tools to study the relative stability of such tautomers. In addition to the relative stability, computational studies permit a direct analysis of the physical and chemical properties of the molecules.

II.1. *Geometrical Parameters*

The internal coordinates describe the position of the atoms in terms of distances (A˚), angles (˚), and torsion angle (˚) concerning an origin atom. The purpose of

this investigation is to study the structure and relative stability of six tautomeric forms of MBPH. The optimized DFT geometry by B3LYP/6-311++G(d,p) of the tautomers with atom numbering is shown in Figures 4-8. By the relaxation of all parameters, the calculations converge to optimize geometries, which correspond to true energy minimum, as revealed by the lack of imaginary frequencies in the vibrational mode calculation. Also, the geometrical parameters have various applications in the explanation of the physicochemical properties of intramolecular hydrogen bonds (IHB) in the system investigated here, and these parameters are represented as follows:

N_1-N_2, N_3-N_4, C_1-N_1, C_2=N_4, C_1-C_2, N_2-H_1, N_3-C_9, N_2-C_6, bond lengths, N_1…H_8 bond distance, N_4-C_2-C_1 and N_3…H_8-N_1 angles for tautomer **(1a)** (Figure 4), for **(1b)** tautomer these parameters are observed beside O_1-H_{13}, O_1-C_{15}, C_{15}-H_{11}, C_{15}-C_2, C_1-H_{14}, N_2-H_{12} bond lengths, N_1……H_{13} bond distance, N_1-C_1-C_2, and C_{15}-O_1-H_{13} angles as shown in Figure 5, also some geometrical parameters are shown for tautomers (**1c & 1d**) as shown in Figure 6, the structural parameters for **(1e)** confirm its reactivity as shown in Figure 7. Also, the geometrical parameters such as bond length (A˚), bond angles (˚), and torsion angles (˚) were investigated to shed more light on the stability of tautomer **(1f)** (Figure 8).

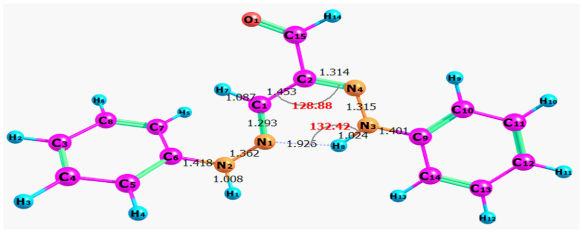

(1a) at DFT/ B3LYP/6311G(d,p)

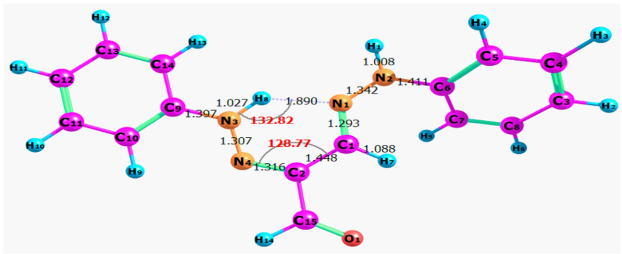

(1a) at DFT/ B3PW91/6311G(d,p)

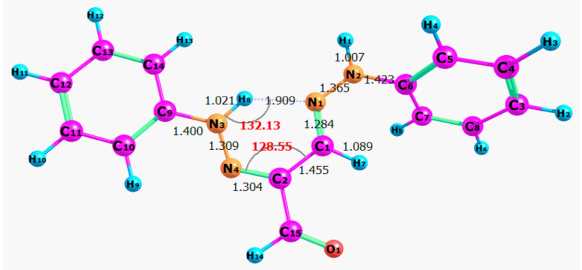

(1a) at DFT/ WB97XD/6311G (d,p)

Figure 4. Some geometrical parameters of the tautomer (1a) were calculated by different DFT methods using the Chemcraft program to visualize the results with intramolecular H-bonds.

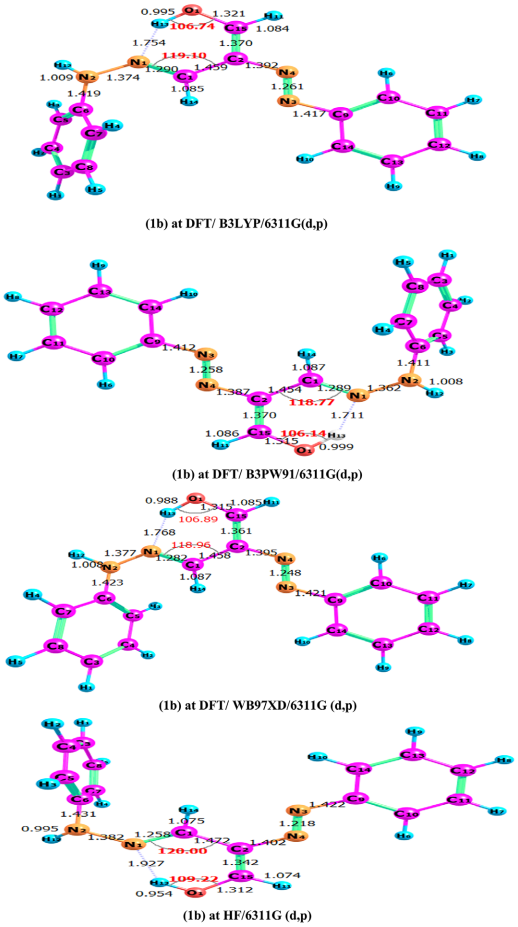

Figure 5. Some geometrical parameters of the tautomer (1b) were calculated by different HF and DFT methods using a Chemcraft program to visualize the results with an intramolecular H-bond.

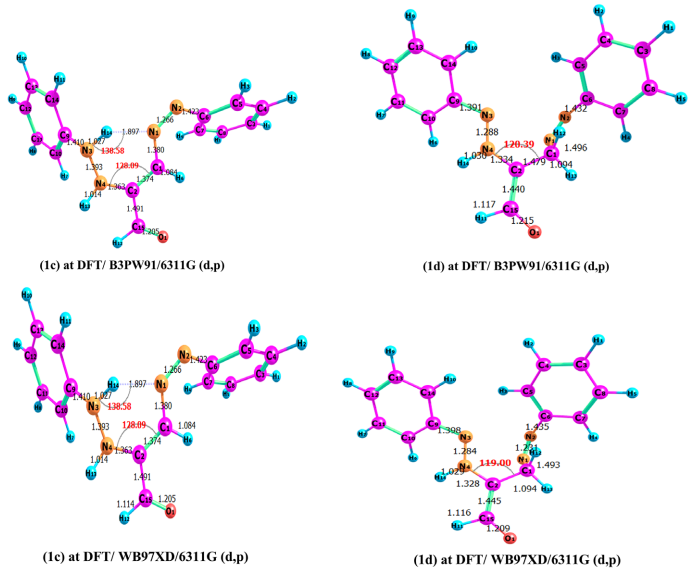

Figure 6. Some geometrical parameters of the tautomers (1c) & (1d) were calculated by DFT methods using a Chemcraft program to visualize the results with intramolecular H-bonds.

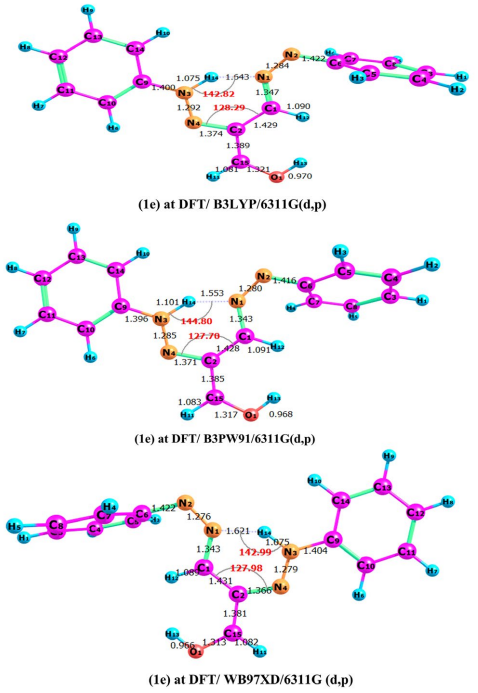

Figure 7. Some geometrical parameters of the tautomer (1e) were calculated by different DFT methods using a Chemcraft program to visualize the results with intramolecular H-bonds.

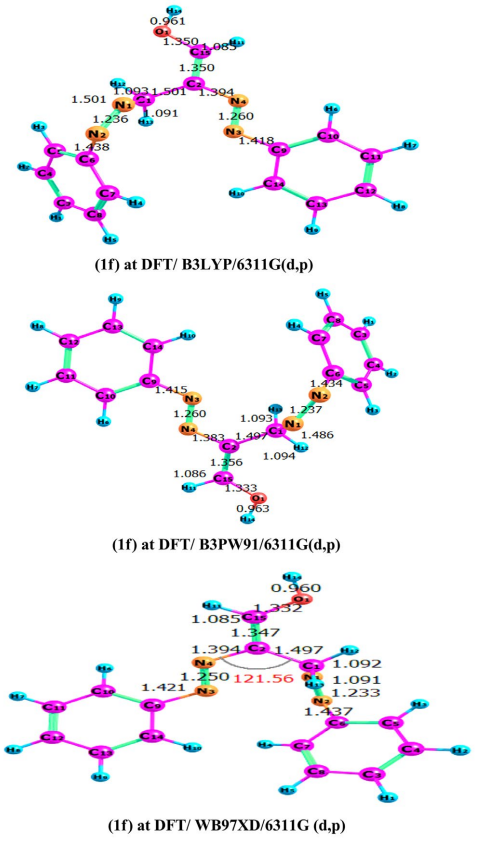

Figure 8. Some geometrical parameters of the tautomer (1f) were calculated by different DFT methods using a chem craft program to visualize the results.

Table 1. Self-consistent field energy, dipole moment, and reactivity parameters of MBPH tautomers calculated by DFT/B3LYP/6-311G(d,p), DFT/B3PW91/6-311G(d,p), DFT/WB97XD/6-311G(d,p), and HF/6-311G(d,p), respectively.

Level of Theory/Parameters	Isomer					
	(1a)	(1b)	(1c)	(1d)	(1e)	(1f)
DFT/B3LYP/6-311G(d,p)						
E (*a.u*)	−874.4050	−874.3869	−874.3597	−874.3466	−874.3350	−874.3470
Dipole moment (*Debye*)	4.4540	2.6793	2.2159	4.4890	4.4650	3.6124
E_{HOMO} (eV)	−5.5950	−5.5615	−5.6061	−5.6665	−4.8916	−5.7144
E_{LUMO} (eV)	−2.0800	−1.8964	−2.8531	−2.7102	−3.3130	−2.0439
ΔE (eV)	3.5152	3.6651	2.7530	2.9562	1.5785	3.6706
IP = ($-E_{HOMO}$)	5.5950	5.5615	5.6061	5.6665	4.8916	5.7144
EA = ($-E_{LUMO}$)	2.0800	1.8964	2.8531	2.7102	3.3130	2.0439
Hardness (η) = (IP − EA)/2	1.7575	1.8326	1.3765	1.4782	0.7893	1.8353
Softness ($1/\eta$)	0.5690	0.5457	0.7264	0.6765	1.2669	0.5449
electronegativity index χ = IP + EA/2	3.8375	3.7290	4.2146	4.1884	4.1023	3.8792
Chemical potential (μ) = $-\chi$	−3.8375	−3.7290	−4.2146	−4.1884	−4.1023	−3.8792
Electrophilicity (ω = $2/2\eta$)	4.1896	3.7938	6.4545	5.9341	10.661	4.0995
Nucleophilicity = E_{HOMO} + 9.12	3.5250	3.5585	3.5140	3.4540	4.2290	3.4060
DFT/B3PW91/6-311G(d,p)						
E (a.u)	−874.0674	−874.0358	−874.0542	−873.9948	−873.9859	−874.0124
Dipole moment (Debye)	6.5144	2.7640	4.5591	4.5931	4.2447	5.3278
E_{HOMO} (eV)	−5.6777	−5.5884	−5.6306	−5.8099	−4.8461	−6.1022
E_{LUMO} (eV)	−2.2782	−1.9298	−2.1233	−2.6515	−3.0779	−2.2874
ΔE (eV)	3.3996	3.6586	3.5073	3.1584	1.7682	3.8148
IP= ($-E_{HOMO}$)	5.6777	5.5884	5.6306	5.8099	4.8461	6.1022
EA= ($-E_{LUMO}$)	2.2782	1.9298	2.1233	2.6515	3.0779	2.2874
Hardness (η) = (IP − EA)/2	1.6998	1.8293	1.7537	1.5792	0.8841	1.9074
Softness ($1/\eta$)	0.5880	0.5467	0.5702	0.6332	1.1310	0.5242
electronegativity index χ = IP + EA/2	3.9783	3.7088	3.8770	4.2307	3.9620	4.1948
Chemical potential (μ) = $-\chi$	−3.9783	−3.7088	−3.8770	−4.2307	−3.9620	−4.1948
Electrophilicity (ω = $2/2\eta$)	4.9150	3.7707	4.2854	5.6670	8.8784	4.6126
Nucleophilicity = E_{HOMO} + 9.12	3.4420	3.5316	3.4894	3.3110	4.2739	3.0178
DFT/WB97XD/6-311G(d,p)						
E (a.u)	−874.013	−874.0716	−874.0466	−874.0311	−874.0128	−874.0538
Dipole moment (*Debye*)	4.0680	2.5797	1.9549	4.9540	4.8190	5.1710
E_{HOMO} (eV)	−7.4620	−7.4595	−7.4285	−7.6195	−6.5316	−8.0065
E_{LUMO} (eV)	−0.0201	−0.0351	−1.1228	−0.8338	−1.3524	−0.3437
ΔE (eV)	7.2609	7.4244	6.3057	6.7858	5.1792	7.6628
IP = ($-E_{HOMO}$)	7.4620	7.4595	7.4285	7.6195	6.5316	8.0065
EA = ($-E_{LUMO}$)	0.0201	0.0351	1.1228	0.8338	1.3524	0.3437
Hardness (η) = (IP − EA)/2	2.8945	3.7122	3.1529	3.3929	2.5896	3.8314
Softness ($1/\eta$)	0.3454	0.2693	0.3172	0.2947	0.3862	0.2610

Continued

electronegativity index χ = IP + EA/2	3.7411	3.7473	4.2757	4.2267	3.9420	4.1751
Chemical potential (μ) = $-\chi$	−3.7411	−3.7473	−4.2757	−4.2267	−3.9420	−4.1751
Electrophilicity ($\omega = 2/2\eta$)	2.4177	1.8914	2.8992	2.6327	3.0003	2.2748
Nucleophilicity = E_{HOMO} + 9.12	1.6580	1.6605	1.6915	1.5005	2.5884	1.1135
HF/6-311G(d,p)						
E (a.u)	−868.9400	−868.9230	−868.9450	−868.8644	−868.9160	−868.9110
Dipole moment (*Debye*)	3.2810	2.3210	2.7920	4.5550	1.5000	5.2720
E_{HOMO} (eV)	−7.8080	−7.9520	−7.7510	−7.6200	−8.0520	−8.4110
E_{LUMO} (eV)	2.0190	2.1780	1.7710	1.2220	2.2230	1.9120
ΔE (eV)	9.8264	10.1300	9.5220	8.8421	10.2751	10.3227
IP = ($-E_{HOMO}$)	7.8080	7.9520	7.7510	7.6200	8.0520	8.4110
EA = ($-E_{LUMO}$)	2.0190	2.1780	1.7710	1.2220	2.2230	1.9120
Hardness (η) = (IP − EA)/2	2.8945	2.8870	2.9755	3.1990	2.9145	3.2495
Softness ($1/\eta$)	0.3455	0.3463	0.3361	0.3222	0.3431	0.3077
Electronegativity index χ = (IP + EA)/2	4.9135	5.0650	4.7610	4.4210	5.1375	5.1765
Chemical potential (μ) = $-\chi$	−4.9135	−5.0650	−4.7610	−4.4210	−5.1375	−5.1765
Electrophilicity ($\omega = 2/2\eta$)	6.3717	6.7976	3.8747	3.0548	6.8931	4.1237
Nucleophilicity = E_{HOMO} + 9.12	1.3120	1.1680	1.3690	1.5200	1.0680	0.7090

Stable, reactive.

All the three DFT methods used in the optimization: DFT/B3LYP, DFT/B3PW91, and DFT/WB97XD with the same basis set, predict that among the six tautomeric forms, the diazo-1-enyl-1-ol form **(1e)** is the most reactive one whereas, the phenyldiazenyl-3-(2-phenylhydrazono)-propane-1-ol **(1f)** found to be the most stable one, Figure 8. and all these methods favor the stability orders as 1f ≥ 1b > 1a > 1d > 1c > 1e, 1f ≥ 1b > 1c > 1a > 1d > 1e and 1f ≥ 1b > 1a >1d > 1c > 1e, respectively. The order of stability obtained by the three DFT methods coincides well, with the most stable tautomer and the most reactive one (Table 1). These results are consistent with the energy gap obtained from the optimization of the conformer (**1e**) with DFT methods. Moreover, the lowering in the HOMO and LUMO energy gap explains the eventual charge transfer interactions that take place within the molecule.

II.2. *Mulliken population analysis*

The bonding capability of a molecule depends on the electronic charge on the chelating atoms. The Mulliken population analysis obtained the atomic charge values [38]. Mulliken analysis is the most common population analysis method. Mulliken atomic charge calculation has a significant role in applying quantum chemical calculations to molecular systems because atomic charges affect some properties of molecular systems including dipole moment which reflects the molecular charge distribution and acts as a vector in three dimensions. Therefore, it can be used as a descriptor to depict the charge movement across the molecule. It

also has been used to describe the electrostatic potential surfaces [39]-[41]. The total atomic charge values of **(1f)** obtained **by** Mulliken population analysis in the applied methods are listed in Table 2 all the hydrogen atoms have a net positive charge. The obtained atomic charge shows that the charges on the more stable tautomer's C1, C2, C8, C18, and C29 atoms are positively charged as they are adjacent to electron acceptor nitrogen atoms. In contrast, the remaining carbons and nitrogen atoms are negatively charged. The results suggest that the atoms bonded to the hydrogen atom and all oxygen atoms are electron acceptors, and indicate the charge transfer from O to H. On the other hand, the hydrogen-bonding length of N4-N3-H…N1-N2 in tautomer **(1a)** is larger than that of C-O-H…N1-N2. in tautomer **(1b)**. This shows that the charge on the O atom of the H-O bond is less than that on N atom of the N3-H bond in the molecule. At the same time, H34 is more acidic due to more positive charge. As expected, the results show that the nitrogen atom (N4) charge in the imine group is the more negatively charged one. They are considering the applied method used in the atomic charge calculation. Continuously, Table 3 shows the Mulliken population analysis of tautomer **(1e)** calculated at HF/6-311G(d,p), DFT/B3LYP/6-311G(d,p), DFT/B3PW91/6-311G(d,p) and DFT/WB97XD/6-311G(d,p) which confirm the charge transfer and from this point of view the results reflect the reactivity of tautomer **(1e)** and the stability of the tautomer **(1f)**, one can conclude that the computed charges are in harmony with the energy gaps tabulated in Table 1.

Table 2. Mulliken atomic charges of tautomer **(1f)** calculated by HF/6-311G(d,p), DFT/B3LYP/6-311G(d,p), DFT/B3PW91/6-311G(d,p) and DFT/WB97XD/6-311G(d,p) respectively.

	Atom	Calculated Method			
		HF	Charge/DFT/B3LYP	Charge/DFT/B3PW91	Charge/DFT/WB97XD
1	C	0.057048	0.073755	0.047159	0.017179
2	C	0.053104	0.036765	0.045487	0.031355
3	N	−0.164662	−0.122997	−0.185695	−0.160447
4	N	−0.580637	−0.317974	−0.432116	−0.435756
5	C	−0.175395	−0.093650	−0.139088	−0.152116
6	C	−0.090516	−0.093903	−0.126341	−0.127716
7	C	−0.151101	−0.051683	−0.109263	−0.124656
8	C	0.177524	0.066421	0.077230	0.079526
9	C	−0.170995	−0.075880	−0.118448	−0.138967
10	C	−0.101567	−0.107879	−0.140992	−0.138669
11	H	0.107771	0.089295	0.116468	0.119815
12	H	0.113939	0.092398	0.119161	0.123043
13	H	0.097177	0.097545	0.102494	0.104848
14	H	0.104401	0.070694	0.119825	0.113646
15	H	0.110960	0.082217	0.115592	0.120178
16	N	−0.244860	−0.170849	−0.226444	−0.200961
17	N	−0.267627	−0.204485	−0.227480	−0.206215

Continued

18	C	0.078805	0.017186	0.033237	0.027140
19	C	−0.040487	−0.016570	0.034307	−0.050775
20	C	−0.120540	−0.096326	−0.123671	−0.128928
21	C	−0.095853	−0.078341	−0.100006	−0.107334
22	C	−0.117843	−0.091789	−0.118521	−0.124305
23	C	−0.072912	−0.040977	−0.070557	−0.078631
24	H	0.136881	0.106840	0.132830	0.136579
25	H	0.128596	0.101548	0.133074	0.138244
26	H	0.129739	0.102465	0.133588	0.138683
27	H	0.127471	0.103335	0.131863	0.137188
28	H	0.129074	0.119816	0.127932	0.133036
29	C	0.289137	0.144048	0.159710	0.164306
30	O	−0.680627	0.466633	−0.501802	−0.520232
31	H	0.170540	0.130662	0.166895	0.173612
32	H	0.133678	0.091733	0.134209	0.130732
33	H	0.349687	0.226486	0.268810	0.281571
34	H	0.580091	0.276727	0.489166	0.525024

Table 3. Mulliken atomic charges of tautomer **(1e)** calculated by HF/6-311G(d,p), DFT/B3LYP/6-311G(d,p), DFT/B3PW91/6-311G(d,p) and DFT/WB97XD/6-311G(d,p) respectively.

	Atom	Calculated Method			
		HF	Charge/DFT B3LYP	Charge/DFT/B3PW91	Charge/DFT/WB97XD
1	C	0.037158	0.038812	0.043780	0.015076
2	C	0.000101	0.030511	0.038686	0.017524
3	N	−0.199493	−0.187717	−0.206070	−0.185692
4	N	−0.472338	−0.314944	−0.340886	−0.339408
5	C	0.129404	−0.091283	−0.101101	−0.112910
6	C	−0.077379	−0.093191	−0.105727	−0.107538
7	C	−0.094418	−0.051430	−0.061299	−0.074947
8	C	0.158042	0.057649	0.065920	0.066025
9	C	−0.131762	−0.078494	−0.086226	−0.103755
10	C	−0.086394	−0.105163	−0.117780	−0.116399
11	H	0.091745	0.092316	0.103436	0.105585
12	H	0.095975	0.094145	0.105257	0.107793
13	H	0.104421	0.097399	0.111288	0.114100
14	H	0.064906	0.072104	0.091432	0.080573
15	H	0.089321	0.088629	0.099299	0.101949
16	N	−0.252332	−0.170849	−0.283654	−0.271211
17	N	−0.151124	−0.192865	−0.212480	−0.172721
18	C	0.208413	0.159363	0.170318	0.166106

Continued

19	C	−0.055709	−0.037167	−0.038398	−0.052091
20	C	−0.083959	−0.091430	−0.104182	−0.106592
21	C	−0.097888	−0.085664	−0.095401	−0.101317
22	C	−0.087445	−0.093922	−0.105637	−0.108170
23	C	−0.124962	−0.111375	−0.123413	−0.129568
24	H	0.132395	0.120179	0.135246	0.138407
25	H	0.116551	0.106843	0.117397	0.123594
26	H	0.113968	0.103996	0.114895	0.121118
27	H	0.116886	0.106059	0.116445	0.123260
28	H	0.113499	0.106455	0.119344	0.124858
29	C	0.272978	0.141411	0.139320	0.143051
30	O	−0.518449	−0.381362	−0.385862	−0.386186
31	H	0.136603	0.125589	0.135981	0.141736
32	H	0.164802	0.136657	0.152880	0.155291
33	H	0.317227	0.237620	0.240469	0.247311
34	H	0.326036	0.252603	0.266726	0.275149

III. Frontier Molecular Orbitals

Frontier orbitals (HOMO and LUMO) are the main participants in electronic transitions, and their energy gap depicts the reactivity [42]. Analysis of the frontier molecular orbitals by computational methods is an elegant way to explain the reactivity and electronic transitions within molecules [43]. To evaluate the energetic behavior of the title compounds, we carried out the calculations for six isomers of mesoxaldehyde-1,2-bis phenylhydrazone, The frontier molecular orbitals (HOMOs/LUMOs) along with corresponding energies of the tautomers **(1a-1f)** were explored at the HF/6-311G(d,p) and DFT (B3LYP, PW91and WB97XD/6-311G(d,p) levels of theory are presented in **Table 1**. The plots of frontier molecular orbitals for mexoxadehyde. Energy gaps for the highest occupied and the lowest unoccupied molecular orbitals were calculated using the equation: Egap = $E_{LUMO} - E_{HOMO}$. Increased LUMO energy level and decreased HOMO energy level result in a higher HOMO-LUMO gap. Higher HOMO-LUMO gap corresponds to higher kinetic stability, thus, lower chemical reactivity [44]-[46]. That is, a small interval between HOMO-LUMO implies low kinetic stability and high chemical reactivity, as it is energetically favorable to add electrons to a LUMO and to extract electrons from a HOMO. Among many others, the energy difference between HOMO and LUMO has been used to predict the activity and intramolecular charge transfer in organic molecules with conjugated Π bonds [47] [48]. Chemical bonds are a source of energy and the movement of molecules in the space is kinetic energy. The vibrations and rotations of molecules are another source of chemical energy along with the chemical reaction, which is a rearrangement of atoms. The energy

gap between HOMO and LUMO represents the stability of structures and helps to characterize some significant issues including the kinetic stability as well as chemical reactivity of the molecule [44]. A molecule with a small frontier orbital gap is more polarizable and is generally associated with a high chemical reactivity as well as low kinetic stability [49]. The conjugated molecules are characterized by a small highest occupied molecular orbital-lowest unoccupied molecular orbital (HOMO-LUMO) separation. From Table 1, it has been found that gap (HOMO-LUMO) of the tautomer **(1f)** is greater than the gap (HOMO-LUMO) relative to all the other tautomers with all the method used; therefore, it is the most stable one. The frontier orbitals (HOMO and LUMO) of the most reactive tautomer **(1e)** and the most stable one **(1f)** are shown in Figure 9 and Figure 10, respectively.

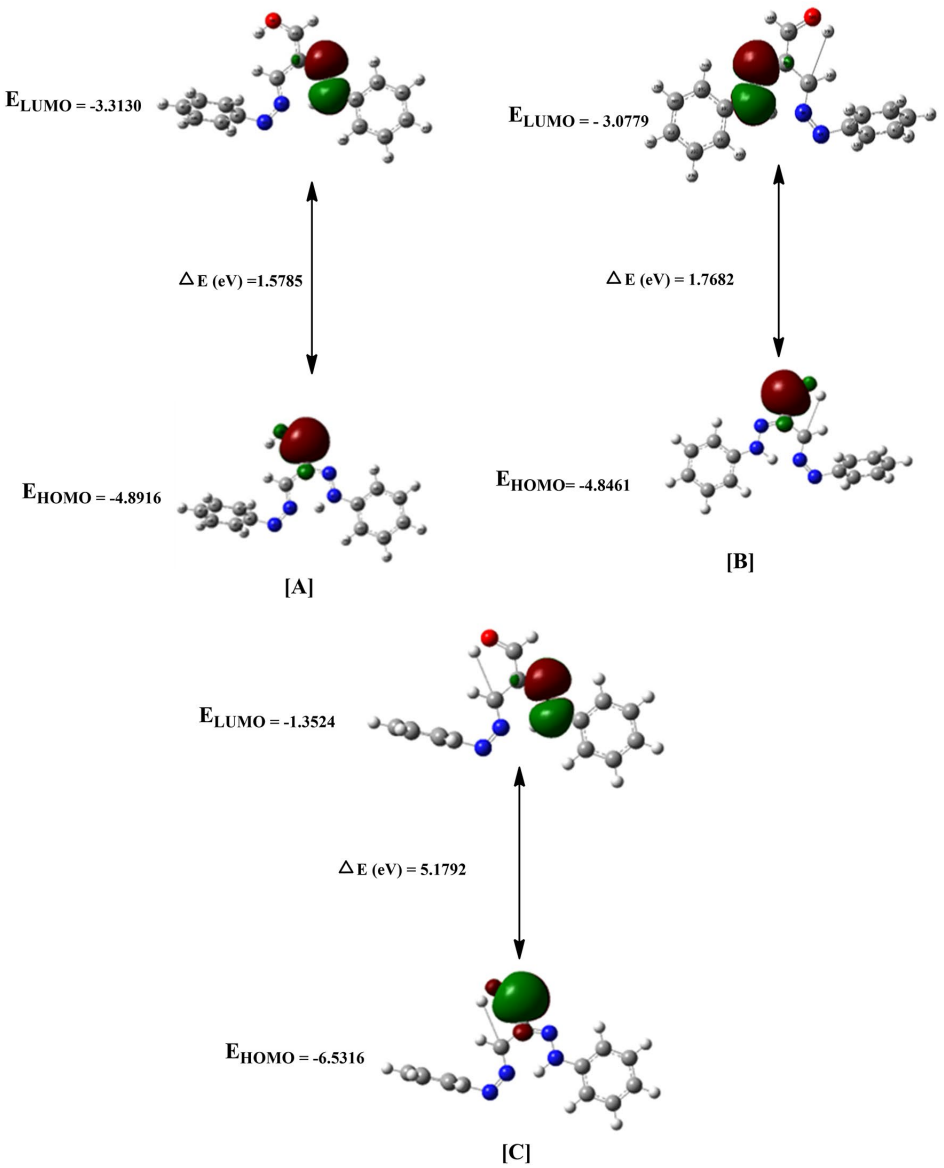

Figure 9. Calculated HOMO-LUMO plot of tautomer (1e) with B3LYP/6-311G(d,p) [A], DFT/B3PW91/6-311G(d,p) [B] and DFT/WB97XD/6-311G(d,p) respectively.

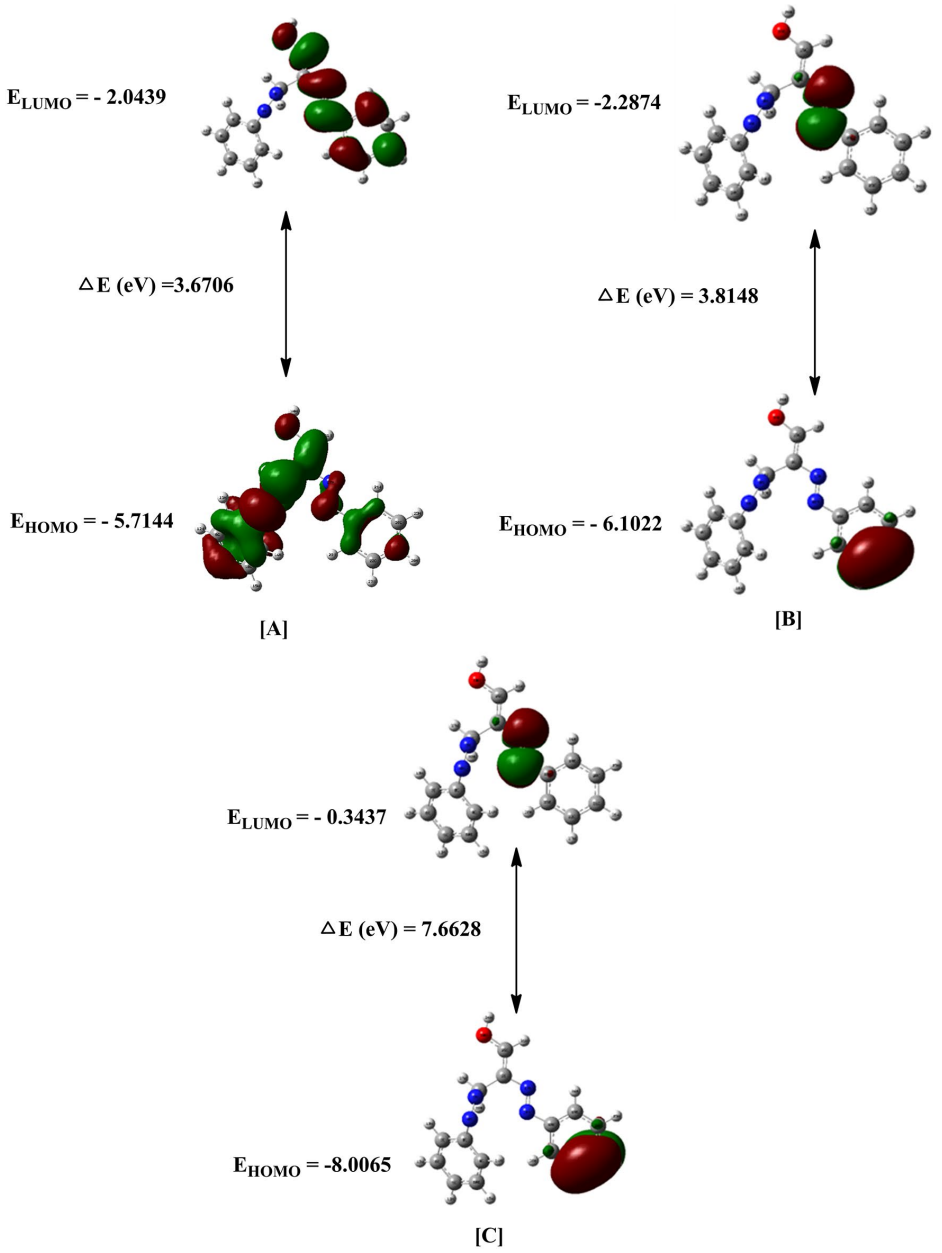

Figure 10. Calculated HOMO-LUMO plot of tautomer (1f) with B3LYP/6-311G(d,p) [A], DFT/B3PW91/6-311G(d,p) [B] and DFT/WB97XD/6-311G(d,p) respectively.

Density functional theory has been successful in providing insights into chemical reactivity and selectivity in terms of global parameters, like electronegativity, hardness, and softness [50]. The concept of hardness/softness is related to the reactivity of the molecules, and it is a property that measures the extent of chemical reactivity to which the addition of a charge stabilizes the system. Molecules with a large HOMO-LUMO energy gap are called "hard" and those with a small HOMO-LUMO energy gap are called "soft". The hardness vs softness of the tautomers of tittle compound calculated at HF and DFT with the three different methods applied in this study are listed in Table 1. DFT showed accurate results

with B3LYP/6-311G(d,p), B3PW91/6-311G(d,p) and WB97XD/6-311G(d,p), the tautomer **(1f)** more stable than (**1b)** are the most stable where their hardness values calculated at DFT/B3LYP/6-311G are 1.8353 and 1.8326 respectively which are high values, these results are consistent with the LUMO-HOMO band gaps of the tautomers (**1f) & (1b)** are 3.6706 and 3.6651 respectively. On the other hand, the reactive tautomer is **(1e)** which showed the high value of the softness 1.2669 **which** consistent with its **LUMO**-HOMO band gap 1.7682, which confirm its reactivity**.** Furthermore, the electrophilicity index (ω) is a measure of the energy stabilization that occurs when the system acquires an additional charge from the environment [51]-[54], increases the electronegativity of tautomer **(1e)**, contributing to lower hardness and higher electrophilicity index 10.661**.** Also, the chemical potential provides a global reactivity index and is related to charge transfer from a system of higher chemical potential to one of lower chemical potential. Electronegativity is the power to attract electrons, and it is related directly to all above properties mentioned in Table 1. Furthermore, there are many attempts to define a nucleophilicity index, simple index was chosen for the nucleophilicity (N) which explains the maximum number of electrons that an electrophile can acquire, based on the HOMO energy, within DFT calculations, explaining the reactivity of the organic material towards electrophiles [55]-[57]. The simple nucleophilicity index (N) is defined as $N = E_{HOMO}$ (ev) + 9.12 (ev), where −9.12 is the energy of the HOMO of tetracyano ethylene (TCE), this nucleophilicity scale is referred to TCE and taken as a reference because TCE exhibits the lowest HOMO energy (=−9.12 eV). From the results depicted in Table 1 we can conclude that, all the tautomers of MBPH calculated at HF/6-311G(d,p), DFT/B3LYP/6-311G(d,p), DFT/B3PW91/6-311G(d,p), and DFT/WB97XD/6-311G(d,p), with high electrophilicity index (ω) and small value of nucleophilicity index is considered to be more likely attacked by a nucleophile, which is in agreement with the suggested mechanisms for the synthesized of heterocyclic compounds from the target compound in this article. Also, the high value of the chemical potential confirms our conclusion.

IV. MEP Surface Mapping

Molecular electrostatic potential (MESP) diagram has been also used to predict the reactive sites for electrophilic and nucleophilic attack, as well as hydrogen bonding interaction [58]-[60], We have reported and plotted the MEP surface mapping, alpha density, and total density of the MEP of more reactive tautomer **(1e)** calculated using Gaussian 09 program with HF/6-311G(d,p), DFT/B3LYP/6-311G(d,p), DFT/B3PW91/6-311G(d,p), and DFT/WB97XD/6-311G(d,p), The MEP surface provides us with net electrostatic effect caused due to total charge distribution. It also provides a useful tool to know the relative polarity of the molecule [61]. The surface is color-coded as per the electrostatic potential (red is more electron-rich and blue is more electron-poor area). The total electron density plot of the tautomer (**1e**) shows a uniform distribution. The order in the increase of the electrostatic potential as per color code will follow as red < orange < yellow <

green [62]. At least we can conclude that the investigated molecule has several sites for electrophilic as well as nucleophilic attacks, as shown in MEP surface mapping (Figure 11).

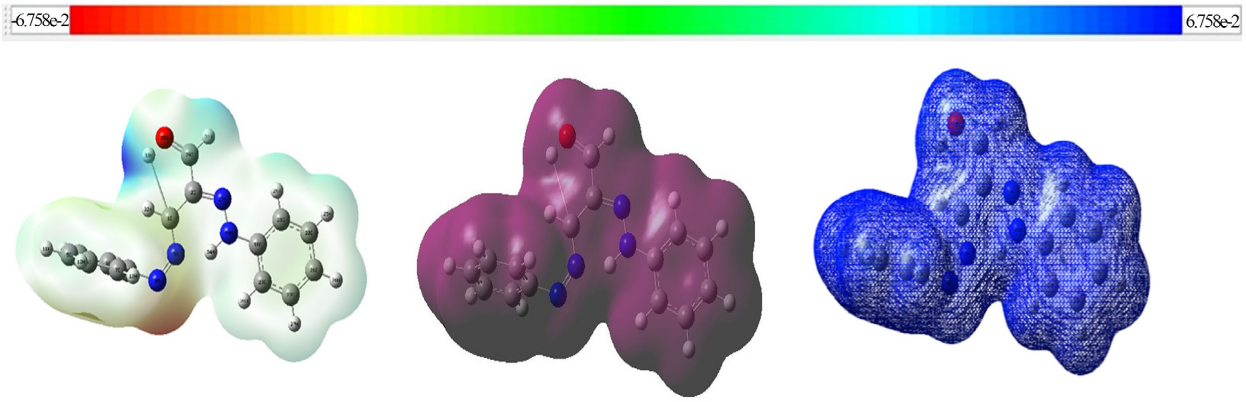

Figure 11. MEP, alpha density, and total density of the tautomer (**1e)** using Gaussian 09 package.

However, it can be seen from the ESP mapping of tautomer **1f** (Figure 12), that the negative ESP is localized more over the molecules and is reflected as a yellowish blob. Different values of the electrostatic potential on the surface are indicated by different colors. Potential increases are listed as red < orange < yellow < green < blue. On the molecular electrostatic potential, negative regions (red and yellow) are associated with electrophilic reactivity, and positive areas (blue) are associated with nucleophilic reactivity. It appears that the negative charge covers the carbonyl group and the positive region is above the remaining groups. The highest electronegativity is located in the carbonyl group.

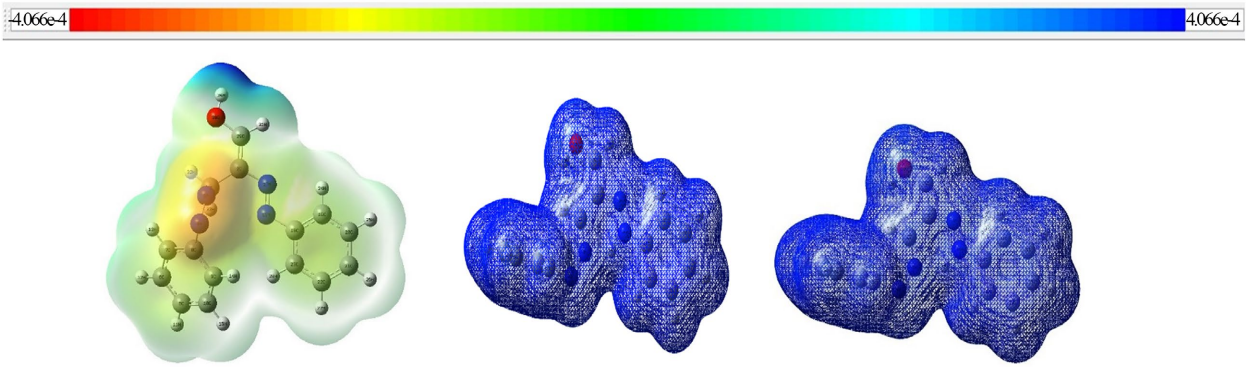

Figure 12. MEP, alpha density, and total density of the tautomer **(1f)** using Gaussian 09 package.

The lines drawn in the contour map clearly show the low electron density in the title molecule (Figure 13). The red color dominating area is found to be highly negative where the nitrogen and the oxygen atoms are located, and other colored parts signify the positive region of the molecule. In the case the three carbon atoms of the tautomers **(1a), (1e),** and **(1f)** are highly positive, more positive than any other carbon atom in the molecule.

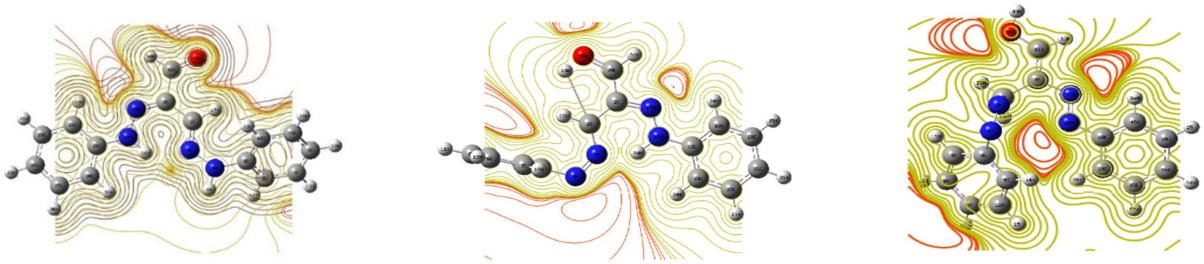

(1a) (1e) (1f)

Figure 13. Contour maps of **(1a), (1e),** and **(1f)** tautomers using the Gaussian 09 package.

V. Thermochemistry analysis:

The computed vibration frequency of the six tautomers of mesoxaldehyde, using HF, B3LYP/6-311G(d,p), B3PW91/6-311G(d,p), and WB97XD/6-311G(d,p), shows some thermodynamic parameter values reflecting molecular polarities, reactivity, and the stability of the molecule. To confirm this, the thermodynamic parameters of tautomer **(1e & 1f)** are tabulated in Table 4, which shows that. Standard enthalpies of formation are evaluated using calculated energies, zero-point vibration energy (ZPVE), plus thermal contributions (to 298 K). The ZPVE corrects the calculated total energy. We found the energy values were slightly dependent on the different methods used for the optimization, and some differences in the relative thermodynamic stability and reactivity of the tautomers were observed. The restricted Hartree-Fock (RHF) method showed a good correlation with the results obtained from the frontier molecular orbitals and the energy gaps.

Table 4. Thermodynamic parameters of the tautomer (1e & 1f) calculated by HF/6-311G(d,p), DFT/B3LYP/6-311G(d,p), DFT/B3PW91/6-311G(d,p), and DFT/WB97XD/6-311G(d,p).

Parameter	Methods of optimization			
	DFT/B3LYP	DFT/B3PW91	DFT/WB97XD	HF
Most stable tautomer (1e)				
Zero-point vibrational energy (Kcal/Mol)	167.84565	166.38624	168.52607	179.37199
Electronic and zero-point Energies (Hartree)	−874.137748	−873.720749	−873.744236	−868.630011
Electronic and thermal Energies (Hartree)	−874.120652	−873.703637	−873.727297	−868.613747
Electronic and thermal Enthalpies (Hartree)	−874.119708	−873.702693	−873.726353	−868.612803
Electronic and thermal Free Energies (Hartree)	−874.185311	−873.769202	−873.792857	−868.678186
	Methods of optimization			
	DFT/B3LYP	**DFT/B3PW91**	**DFT/WB97XD**	**HF**
Most active tautomer (1f)				
Zero-point vibrational energy (Kcal/Mol)	166.71755	167.40032	169.28107	179.30859
Electronic and zero-point Energies (Hartree)	−874.081345	−873.745664	−873.784027	−868.625242
Electronic and thermal Energies (Hartree)	−874.063958	−873.728400	−873.767026	−868.608962
Electronic and thermal Enthalpies (Hartree)	−874.063014	−873.727455	−873.766082	−868.608018
Electronic and thermal Free Energies (Hartree)	−874.130136	−873.794232	−873.831244	−868.672750

3.2. Chemistry

The nucleophilic and electrophilic activities of mesoxaldehyde, 1,2-bis phenyl hydrazone predicted from the computational studies, attract our attention to the use of it as a starting compound to synthesize different heterocyclic compounds (Scheme 1). The structure of the synthesized compounds was identified using different spectral tools. The intramolecular cyclization of hydrazones using cupric chloride ($CuCl_2$) is a fascinating area of research in organic chemistry. This reaction typically involves forming a cyclic structure by activating the hydrazone with cupric chloride, facilitating the cyclization process. In this article, we design to use MBPH as strating materials for the synthesis of substituted heterocyclic derivatives via the reaction with different hydrazides, followed by intramolecular cyclization. Firstly, mesoxaldehyde was prepared as shown in the literature [17], and the structure was confirmed using different spectral tools (Figure 14).

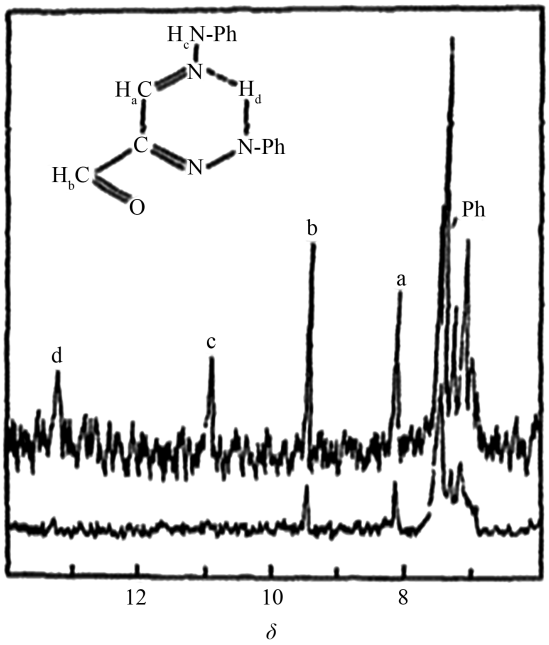

Figure 14. The ^{1}H-NMR spectrum of MBPH before deuteration (upper curve) and after deuteration (lower curve).

The reaction of mesoxaldehyde with thiosemicarbazide or semicarbazide in the presence of acetic acid gives the corresponding thiosemicarbazone or semicarbazone derivatives (Scheme 1). The structure of the thiocarbazone derivative (2) was identified using different spectral tools, the infra-red spectrum (cm^{-1}) showed the presence of the amino group (NH_2) and the imine (NH) at γ = 3583, 3172 respectively, 1660 for (CN) and 1267 for (CS), and no band between 1800 and 1690 cm^{-1} attributed the absence of carbonyl group. The proton nuclear magnetic resonance spectra (^{1}H-NMR) showed the presence of exchangeable NH at δ = 9.33 ppm, the aromatic protons of the phenyl groups appear as a multiplet at δ = 7.19 - 7.89 ppm, the amino group of the carbazone moiety appears as an exchangeable broad

band at δ = 4.55 ppm, also the structure of (2) was confirmed using ^{13}C-NMR and elemental analysis (see experimental). Also, the structure of the semicarbazone derivative (3) showed the same spectral data except for the appearance of a carbonyl band in the infrared spectrum instead of the CS band. Continuously, treatment of the thiocarbazone derivative (2) or the carbazone (3) with an ethanolic solution of cupric chloride gave the corresponding triazole derivatives (4) or (5) through intramolecular cyclization. The structures of each (4) and (5) were identified using different spectral tools and alternative synthesis. For example, the structure of (5) was confirmed using the infrared spectrum which showed two bands at γ = 3421, 3290 cm^{-1} corresponding for NH_2 & NH, 1690 cm^{-1} for (CO), and 1630 cm^{-1} for (CN). The ^{1}H NMR spectra showed a singlet δ = 11.92 ppm exchangeable N-H, δ = 8.32 ppm as a singlet for C-5 triazole proton the amino group appears as a singlet at δ = 7.68 ppm and finally a multiplet at δ = 6.81 - 7.35 for the hydrazide proton and the phenyl ring protons. Also, we can confirm that the cyclization of (2) or (3) to give the corresponding triazole derivatives **(4)** or **(5)**, and acetylation of the triazoles (4) with boiling acetic anhydride gave the corresponding products **(6)**. The structure of 4-((2-acetyl-2-phenylhydrazono) methyl)-2H-1,2,3-triazole-2-carbothioamide **(6)** was confirmed using different spectral tools, the infrared spectrum (cm^{-1}) showed characteristic bands at 3583 (NH_2), 1710 ($COCH_3$), 1660 (CN), 1 270 (CS). ^{1}H NMR ($CDCl_3$): δ (ppm) showed an exchangeable singlet at 8.56 for NH_2, a singlet at 8.32 for C-5 triazole proton, a multiplet at 7.13 - 7.94 for aromatic and hydrazide protons and finally a singlet at 2.04 for the acetyl group protons. On the other hand, acetylation of the thiocarbazone (2) and the carbazone (3) with boiling acetic anhydride gave the corresponding thiadiazol derivative **(7)** and the oxadiazole **(8)** respectively. The thiadiazol **(7)** was separated as yellow needle**s** in good yield (75%). m.p. 257˚C - 258˚C; IR (cm^{-1}, KBr): ν = 3290 (NH), 1710 (*CO*CH_3), 1660 (CN). ^{1}H NMR ($CDCl_3$): δ (ppm) = 9.01 (s, 1H, *NH*COCH3, exchangeable), 8.20 (s, 2H, *NH*-Ph, exchangeable) 6.81 - 7.35 (m, 11H. Ar-H, hydrazide proton), 4.6 (s.1H, C-5 thiadiazol ring), 2.22 (s, 3H, acetyl group), 2.08 (s, 3H, NHCO*CH3*). ^{13}C NMR: δ (ppm) = 169, 167 (2CO), 139 (hydrazide carbon). The oxadiazole **(8)** has revealed the same spectral data as **(7)**, its infra-red spectra. IR (cm^{-1}, KBr) shows ν = 3290 (NH), 1710 (*CO*CH_3), 1610 (CN). ^{1}H NMR ($CDCl_3$): δ (ppm) = 11.01 (s, 1H, *NH*COCH3, exchangeable), 9.20 (s, 2H, *NH*-Ph, exchangeable) 6.81 - 7.35 (m, 11H. Ar-H & hydrazide protons), 4.6 (s.1H, C-5 oxadiazol ring), 2.22 (s, 3H, N-acetyl group), 2.08 (s, 3H, NHCO*CH3*). ^{13}C NMR: δ (ppm) = 169, 167 (2CO), 139 (hydrazide carbon), 138, 128, 128,128, 124, 143 (C Ar-N), 21.6 (CH_3). Treatment of **(7)** or **(8)** with an ethanolic solution of cupric chloride gave the bicyclic compounds **(9**) or **(10)**. Scheme 1, the structure of these products was confirmed by alternative synthesis using a different route as follows: Mesoxaldehyde, 1,2-bis phenyl hydrazone was treated with an ethanolic solution of cupric chloride to give the corresponding triazole **(11)**, which reacted with an acidic solution of thiosemicarbazide or semicarbazide to give the corresponding triazole **(12)** or **(13)** which differ completely

than the triazole **(4)** or **(5)**, the isolated triazoles were confirmed using different spectral tools and elemental analysis.(see experimental section). Acetylation of the triazole **(13)** with boiling acetic anhydride gave the corresponding bicyclo compound which is identical with that obtained from the other route. Finally, it has been found that **(10)** and **(14)**, which were obtained from two different routes, have the same structural formula and were confirmed by using different spectral tools and alternative synthesis. This result confirms that in the first root triazole derivatives **(4)** or **(5)** obtained via intramolecular elimination reaction between C-1&C-2 not between C-2&C-3, and this was confirmed by treatment of MBPH, firstly with an ethanolic solution of cupric chloride to give the corresponding triazole aldehyde **(11)** which reacted with thiosemicarbazide or semicarbazide gave the triazole derivative **(12) & (13)** which differ completely than the other triazoles **(4) or (5)** in their color and melting points (see experimental section), also from the computational study section, we conclude that C1, C2 & C3 of MBPH which calculated using the HF& DFT methods are positively charged, but C3 is the more positively one, so the cyclization preferred to occur between C-1&C-2 not between C-2&C3.

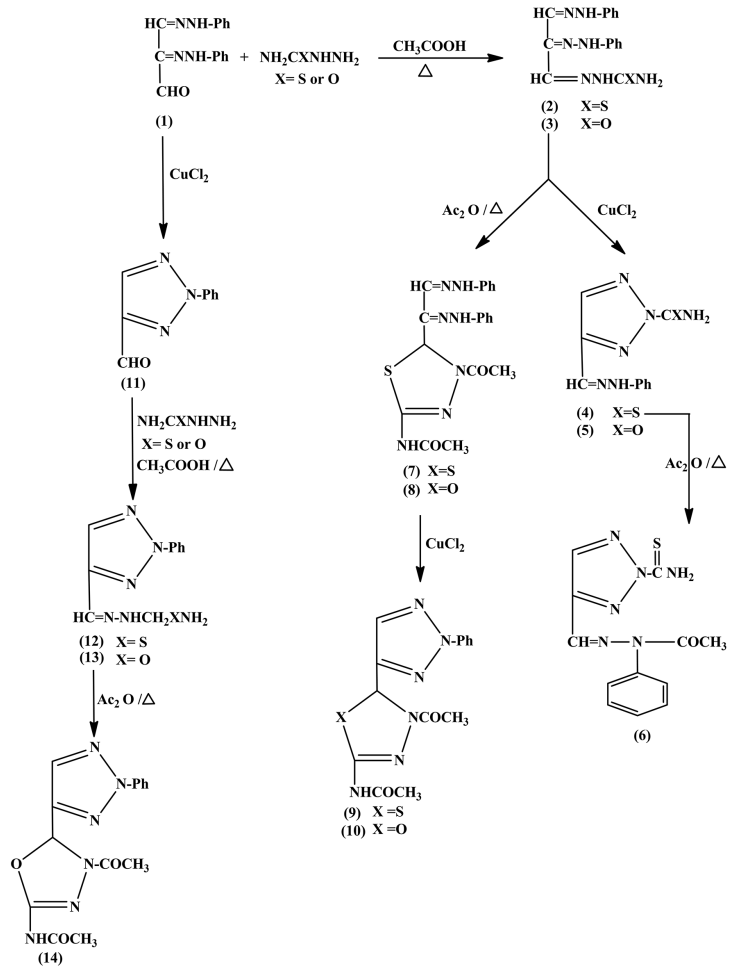

Scheme 1. Synthesis of different heterocyclic compounds from mesoxaldehyde.

4. Experimental

4.1. Chemistry

4.1.1. General Methods

Melting points were carried out on a Tottoli (Büchi) apparatus and were not corrected. IR (KBr) was recorded on a PerkinElmer 580 VB spectrophotometer and on a Camica 250 Hz spectrometer. Microanalyses were performed in microanalytical units, Department of Chemistry, Faculty of Science, Cairo University, Cairo, Egypt. Mass spectra were carried out on Direct Inlet part to mass analyzer on a Thermo Scientific GCMS model ISQ (70 eV El mode), performed at the Regional Center for Mycology and Biotechnology Al-Azhar University, Cairo, Egypt. The nuclear magnetic resonance spectra (1H-NMR & 13C-NMR) for the purified sample in (CDCl3) or (DMSO d6) were obtained using a Joel EAC 500 MHz FT-NMR spectrophotometer (Faculty of Science, Alexandria University, Egypt) and on a Varian Gemini VX-300 MHz spectrophotometer using TMS as an internal standard, (Faculty of Science, Cairo University, Egypt) at the Regional Center for Mycology and Biotechnology (RCMB), Al-Azhar University, Nasr city, Cairo, Egypt. The reaction progress was monitored by thin-layer chromatography (TLC) on silica gel 60 f 254 plates.

4.1.2. Synthesis of the Studied Compounds

Mesoxaldehyde-2,3-bis phenyl hydrazone (1). Prepared as shown in the literature [17].

2,3-bis (2-phenylhydrazono) propylidene)-1-hydrazine carbothioamide (2)

A solution of compound **(1)** (1 g) in 95% ethanol (30 ml) was treated with thiosemicarbazide (1 g), and a few drops of acetic acid. The reaction mixture was heated under reflux for 3 hours, then concentrated and poured onto crushed ice. The separated crude solid was filtered off, washed successively with water, dried, and recrystallized from ethanol to give **(2)** orange-yellow needles. The yield of (**2**) was 77%, m.p. 183˚C - 184˚C; IR (cm^{-1}, KBr): ν = 3583, 3172 (NH_2, NH), 1660 (CN); 1267 (CS). ^{1}H NMR ($CDCl_3$): δ (ppm) = 9.33 (s, 3H, NH, exchangeable), 7.19 - 7.89 (m, 12H, Ar-H & 2 hydrazide protons), 4.55 (br s, 2H, NH_2, exchangeable); ^{13}C NMR ($CDCl_3$): δ (ppm) = 181 (C-1, CS), 128 (C-2), 140 (C Ar-N), 143 (C Ar-N), the other signal carbons of the two phenyl rings appear at 113.9, 122, 129.5 Anal. Calcd for $C_{16}H_{17}N_7S$ (339): C, 56.64; H, 5.01; N, 28.91%. Found: C,56.88; H, 5.40; N, 28.28%.

2,3-bis (2-phenylhydrazono) propylidene)-1-hydrazine carboxamide (3)

A solution of compound **(1)** (1 g) in 95% ethanol (30 ml) was treated with semicarbazide (1 g), and a few drops of acetic acid, the reaction mixture was heated under reflux for 3 hours, then, concentrated and poured onto crushed ice. The separated crude solid was filtered off, washed successively with water, dried, and recrystallized from ethanol to give **(3)** yellow needles. The yield of (**3**) was 70%, m.p. 150˚C - 151˚C; IR (cm^{-1}, KBr): ν = 3470, 3220 (NH2, NH), 1690 (CO); 1660 (CN). ^{1}H NMR ($CDCl_3$): δ (ppm) = 9.33 (s, 3H, NH, exchangeable), 7.19 - 7.89

(m, 12H, Ar-H & 2 hydrazide protons), 4.55 (br s, 2H, NH_2, exchangeable). ^{13}C NMR($CDCl_3$): 169 (CO), 128 (C-2), 140 (C Ar-N), 143 (C Ar-N), the other signal carbons of the two phenyl rings appear at 113.9, 122, 129.5 Anal. Calcd for $C_{16}H_{17}N_7O$ (323): C, 59.44; H, 5.26; N, 30.34%. Found: C, 59.90; H, 5.40; N, 30.28%.

4-((2-phenylhydrazono) methyl)-2H-1,2,3-triazole-2-carbothioamide (4)

Bis phenyl thiocarbazone **(2)** (1.1 mmol) was dissolved in (10 ml) of 1:1 absolute ethanol/acetone mixture in a 100 ml beaker and allowed to stir for 10 minutes. Then, an ethanolic solution of Cu (II)chloride (1.1 mmol) was added dropwise to the stirring mixture. The mixture was stirred for 6 hrs at room temperature after which the precipitate formed was filtered and washed using 40% ethanol and dried in a desiccator over calcium chloride. The product was recrystallized from ethanol as yellow needles. The yield of (**4**) was 60%, m.p. 150˚C - 151˚C; IR (cm^{-1}, KBr): ν = 3421 (NH_2), 3290 (NH), 1270 (CS), 1660 (CN). ^1H NMR ($CDCl_3$): δ (ppm) = 11.92 (s, 1H, N-H, exchangeable), 8.56 (s, 2H, NH_2, exchangeable), 8.32 (s, 1H, C-5 triazole proton), 6.81 - 7.35 (m, 6H, Ar-H & hydrazide protons). C^{13}NMR ($CDCl_3$): δ (ppm) = 174 (CS), 144 (C5-triazole), 143 (Ph-C-N), 130 (C4 triazole), 129, 122, 113 (aromatic ring carbons) 121 (C=N hydrazone moiety). Anal. Calcd for $C_{10}H_{10}N_6S$ (246): C, 48.78; H, 4.07; N, 34.15%. Found: C, 48.90; H, 4.40; N, 34.28%.

4-((2-phenylhydrazono) methyl)-2H-1,2,3-triazole-2-carboxamide (5)

Bis phenyl carbazone **(3)** (1.1 mmol) was dissolved in (10 ml) of 1:1 absolute ethanol/acetone mixture in a 100 ml beaker and allowed to stir for 10 minutes. Then, an ethanolic solution of Cu (II) chloride (1.1 mmol) was added dropwise to the stirring mixture. The mixture was stirred for 6 hrs at room temperature after which the precipitate formed was filtered and washed using 40% ethanol and dried in a desiccator over calcium chloride. The product was recrystallized from ethanol as colorless needles. The yield of (**5**) was 65%, m.p. 120˚C - 121˚C; IR (cm^{-1}, KBr): ν = 3421 (NH_2), 3290 (NH), 1690 (CO), 1630 (CN). ^1H NMR ($CDCl_3$): δ (ppm) = 11.92 (s, 1H, N-H, exchangeable), 8.32 (s, 1H, C-5 triazole proton), 7.68 (s, 2H, NH_2, exchangeable), 6.81 - 7.35 (m, 6H, Ar-H, hydrazide proton). C^{13}NMR ($CDCl_3$): δ (ppm) 164(CO), 144 (C5-triazole), 143 (Ph-C-N), 130 (C4 triazole), 129, 122, 113 (aromatic ring carbons) 121 (C=N hydrazone moiety) Anal. Calcd for $C_{10}H_{10}N_6O$ (230): C, 52.17; H, 4.38; N, 36.50%. Found: C, 52.90; H, 4.40; N, 36.28%.

4-((2-acetyl-2-phenylhydrazono) methyl)-2H-1,2,3-triazole-2-carbothioamide (6)

A mixture of **(4)** (5 mmol), acetic anhydride (10 ml), was heated under reflux for 2 h. The reaction mixture was poured into crushed ice, and the solid that separated was filtered off, washed successively with water, dried, and recrystallized from proper solvent to give **(6)** good yield (75%). m.p. 123˚C - 125˚C; IR (cm^{-1}, KBr): ν = 3583 (NH_2), 1710 ($COCH_3$), 1660 (CN), 1270 (CS). ^1H NMR ($CDCl_3$): δ (ppm) = 8.56 (s, 2H, NH_2, exchangeable), 8.32 (s,1H, C-5 triazole proton), 7.13 -

7.94 (m, 6H. Ar-H, hydrazide proton), (2.04, 3H, acetyl group). ^{13}C NMR: δ (ppm) = 177 (CS), 172 (CO), 145.130 (C_4, C_5 triazole protons), (139, hydrazide carbon), 138, 128, 128, 124, 143 (C Ar-N), 21.6 (CH_3). Anal. Calcd for $C_{12}H_{12}N_6OS$ (288): C, 49.99; H, 4.19; N, 29.15%. Found: C, 49.90; H, 4.40; N, 29.28%.

N-(4-acetyl-5-(1-(2-phenylhydrazono) ethyl)-4,5-dihydro-1,3,4-thiadiazol-2-yl) acetamide (7)

A mixture of **(2)** (5 mmol), acetic anhydride (10 ml), was heated under reflux for 3 h. The reaction mixture was poured into crushed ice, and the solid that separated was filtered off, washed successively with water, dried, and recrystallized from proper solvent to give **(7)** as yellow needles in good yield (75%). m.p. 257˚C - 258˚C; IR (cm^{-1}, KBr): ν = 3290 (NH),1710 ($COCH_3$), 1660 (CN). ^{1}H NMR ($CDCl_3$): δ (ppm) = 9.01 (s, 1H, *NH*COCH3, exchangeable), 8.20 (s, 2H, *NH*-Ph, exchangeable) 6.81 - 7.35 (m, 11H. Ar-H & hydrazide protons), 4.6 (s.1H, C-5 thiadiazol ring), 2.22 (s, 3H, acetyl group), 2.08 (s, 3H, NHCO*CH3*). ^{13}C NMR: δ (ppm) = 169, 167 (2CO), 139 (hydrazide carbon), 138, 128, 128, 128, 124, 143(C Ar-N), 21.6 (CH_3). Anal. Calcd for $C_{20}H_{21}N_7O_2S$ (423): C, 49.99; H, 4.19; N, 29.15%. Found: C, 49.90; H, 4.40; N, 29.28%.

N-(4-acetyl-5-(1-((2,3-bis-phenylhydrazono-ethyl))-4,5-dihydro-1,3,4-oxadiazol-2-yl) acetamide (8)

A mixture of **(3)** (5 mmol), acetic anhydride (10 ml), was heated under reflux for 2 h. The reaction mixture was poured into crushed ice, and the solid that separated was filtered off, washed successively with water, dried, and recrystallized from proper solvent to give **(8)** a good yield (75%). m.p. 223˚C - 225˚C. IR (cm^{-1}, KBr): ν = 3290 (NH), 1710 ($COCH_3$), 1610 (CN). ^{1}H NMR ($CDCl_3$): δ (ppm) = 11.01 (s, 1H, *NH*COCH3, exchangeable), 9.20 (s, 2H, *NH*-Ph, exchangeable) 6.81 - 7.35 (m, 11H. Ar-H, hydrazide proton), 4.6 (s.1H, C-5 oxadiazol ring), 2.22 (s, 3H, N-acetyl group), 2.08 (s, 3H, NHCO*CH3*). ^{13}C NMR: δ (ppm) = 169, 167 (2CO), 139 (hydrazide carbon), 138, 128, 128, 128, 128, 128, 124, 143(C Ar-N), 21.6 (CH_3). Anal. Calcd for $C_{20}H_{21}N_7O_3$ (407): C, 58.97; H, 5.16; N, 24.08%. Found: C, 58.90; H, 5.40; N, 24.28%.

N-(4-acetyl-5-(2-phenyl-2H-1,2,3-triazol-4-yl)-4,5-dihydro-1,3,4-thiadiazol-2-yl) acetamide (9)

Compound **(7)** (1.1 mmol) was dissolved in 10 mL of a 1:1 absolute ethanol/acetone mixture in a 100 mL beaker and stirred for 10 minutes. Then, an ethanolic solution of Cu (II)chloride (1.1 mmol) was added dropwise to the stirring mixture. The mixture was stirred for 6 hrs. at room temperature, after which the precipitate formed was filtered and washed using 40% ethanol and dried in a desiccator over calcium chloride. The product was recrystallized from ethanol as colorless needles. The yield of (**9**) was 60%, m.p. 157˚C - 158˚C; IR (cm^{-1}, KBr): ν = 3440 (NH), 1730 ($COCH_3$), 1660 (CN). ^{1}H NMR ($CDCl_3$): δ (ppm) = 11.92 (s, 1H, *NH*COCH3, exchangeable), 8.00 (s, 1H, C-5 thiadiazol proton), 7.45 - 8.09 (m, 6H, Ar-H, C-5 triazole ring proton), 2.22 (s, 3H, N-acetyl group), 2.08 (s, 3H, NHCO*CH3*). C^{13} NMR(CDCl3): 169, 167(2 C=O), 138, 128, 119 (Aromatic ring

carbons), 145, 52 (C_2&C_5 thiadiazol ring), 132 (C_4, C_5 triazole) Anal. Calcd for $C_{14}H_{14}N_6O_2S$ (330): C, 50.90; H, 4.27; N, 25.44%. Found: C, 50.95; H, 4.40; N, 25.28%.

N-(4-acetyl-5-(2-phenyl-2H-1,2,3-triazol-4-yl)-4,5-dihydro-1,3,4-oxadiazol-2-yl) acetamide (10)

Compound **(8)** (1.1 mmol) was dissolved in (10 ml) of 1:1 absolute ethanol/acetone mixture in a 100 ml beaker and allowed to stir for 10 minutes. Then, an ethanolic solution of Cu (II)chloride (1.1 mmol) was added dropwise to the stirring mixture. The mixture was stirred for 6 hrs at room temperature after which the precipitate formed was filtered and washed using 40% ethanol and dried in a desiccator over calcium chloride. The product was recrystallized from ethanol as colorless needles. The yield of (**10**) was 70%, m.p. 154˚C - 155˚C; IR (cm^{-1}, KBr): ν = 3440 (NH), 1730 ($COCH_3$), 1660 (CN). ^{1}H NMR ($CDCl_3$): δ (ppm) = 11.92 (s, 1H, *NH*COCH3, exchangeable), 8.00 (s, 1H, C-5 oxadiazole proton), 7.45 - 8.09 (m, 6H, Ar-H, C-5 triazole ring proton) 2.22 (s, 3H, N-acetyl group), 2.08 (s, 3H, NHCO*CH3*). C^{13} NMR(CDCl3): 169, 167 (2 C=O), 138, 128, 119 (Aromatic ring carbons) 145, 52 (C_2&C_5 oxadiazol ring) 132 (C_4, C_5 triazole). Anal. Calcd for $C_{14}H_{14}N_6O_3$ (314): C, 53.50; H, 4.45; N, 26.75%. Found: C, 53.95; H, 4.45; N, 26.75%.

2-phenyl-2H-1,2,3-triazole-4-carbaldehyde (11)

Mesoxaldehyde-2,3-bis phenyl hydrazone (1.1 mmol) was dissolved in 10 ml of a 1:1 absolute ethanol/acetone mixture in a 100 ml beaker and stirred for 10 minutes. Then, an ethanolic solution of Cu (II)chloride (1.1 mmol) was added dropwise to the stirring mixture. The mixture was stirred for 6 hours at room temperature, after which the precipitate formed was filtered and washed with 40% ethanol, and then dried in a desiccator over calcium chloride. The product was recrystallized from ethanol as yellow needles. m.p. 178˚C - 179˚C; IR (cm^{-1}, KBr): ν = 1690 (C=O, aldehyde). 1H NMR (CDCl3): δ (ppm) = 9.75 (s, 1H, *H*CO), 7.58 - 8.46 (m, 6H, Ar-H& C-5 triazole ring protons) C^{13} NMR(CDCl3): 185 (CO), 149 (C4 triazole, 139 (C-N), 132 (C5 triazole), 128, 119 (Phenyl ring carbons). Anal. Calcd for $C_9H_7N_3O$ (173): C, 62.42; H, 4.07; N, 24.27%. Found: C, 63.95; H, 4.45; N, 24.75%.

2-phenyl-2H-1,2,3-triazole-4-hydrazine carbothioamide (12)

A solution of compound **(11)** (1 g) in 95%ethanol (30 ml) was treated with thiosemicarbazide (1 g), and a few drops of acetic acid. The reaction mixture was heated under reflux for 3 hours, then, concentrated and poured onto crushed ice. The separated crude solid was filtered off, washed successively with water, dried, and recrystallized from ethanol to give **(12)** colorless needles. The yield of (1**2)** was 77%, m.p. 222˚C - 223˚C; IR (cm^{-1}, KBr): ν = 3470, 3172 (NH_2, NH), 1600 (CN); 1267 (CS). ^{1}H NMR ($CDCl_3$): δ (ppm) = 10.92 (s,1H, N-H, exchangeable), 8.56 (s, 2H, NH_2, exchangeable), 8.32 (s,1H, C-5 triazole proton), 6.81 - 7.35 (m, 6H, Ar-H & hydrazide protons). Anal. Calcd for $C_{10}H_{10}N_6S$ (246): C, 48.78; H, 4.07; N, 34.15%. Found: C, 48.80; H, 4.20; N, 34.25%.

2-phenyl-2H-1,2,3-triazole-4-hydrazine carboxamide (13)

A solution of compound **(11)** (1 g) in 95% ethanol (30 ml) was treated with semicarbazide (1 g), and a few drops of acetic acid. The reaction mixture was heated under reflux for 3 hours, then, concentrated and poured onto crushed ice. The separated crude solid was filtered off, washed successively with water, dried, and recrystallized from ethanol to give **(3)** colorless needles. The yield of (**3**) was 70%, m.p. 240˚C - 241˚C; IR (cm^{-1}, KBr): ν = 3470,3220 (NH2, NH), 1690 (CO); 1600 (CN). ^1H NMR ($CDCl_3$): δ (ppm) 10.92 (s, 1H, N-H, exchangeable), 8.32 (s, 1H, C-5 triazole proton), 8.00 (s, 2H, NH_2, exchangeable), 6.81 - 7.35 (m, 6H, Ar-H, hydrazide proton). Anal. Calcd for $C_{10}H_{10}N_6O$ (230): C, 52.17; H, 4.38; N, 36.50%. Found: C, 52.70; H, 4.20; N, 36.20%.

N-(4-acetyl-5-(2-phenyl-2H-1,2,3-triazol-4-yl)-4,5-dihydro-1,3,4-oxadiazol-2-yl)acetamide (14)

A mixture of **(13)** (5 mmol), acetic anhydride (10 ml), was heated under reflux for 2 h. The reaction mixture was poured into crushed ice, and the solid that separated was filtered off, washed successively with water, dried, and recrystallized from proper solvent to give **(8)** a good yield (75%). The melting point and all the spectral data are shown to be identical with the compound **(10).**

4.2. Computational Methods

All calculations for the studied compounds were performed by using the Gaussian 09 software package [22] with a Pentium IV processor personal computer. DFT performed the calculations by using Becke's three-parameter exchange functional [23] with a hybrid function using the Lee, Yang, and Parr (LYP) correlation functional [24] [25] B3LYP method, Perdew and Wang's 1991 (PW91) [26] and the range separated hybrid WB97XD [27] Energy optimization of the ground states of the compounds was performed by using the split-valence double zeta basis set 6-311G with two polarized basis functions (d and p), for which the p-type orbital was added to all hydrogen atoms as well as a diffuse function. The gas-phase-optimized structure of the most stable isomer was thus classified as its starting geometry, complete geometry optimization without restriction. The geometries were optimized by minimizing the energies concerning all geometrical parameters. Gauss-View and Chem craft programs [28] [29] were used to get computation results to visualize the optimization structures and draw the frontier molecular orbital (FMOs) and molecular electrostatic potential (MEP) maps [30].

5. Conclusion

In this article, the optimized geometries of six possible tautomers of mesoxaldehyde 2,3-biphenyl (MBPH) **(1)** have been studied in the gas phase. The different conformers of the compound were studied using the B3LYP functional with a 6-311G(d,p) basis set, and the most stable conformer with the minimum energy was identified. This conformer was then used for further computations. Determination of the energy gap by using HOMO and LUMO energy values and identification of

electrophilic and nucleophilic regions. Thermodynamic properties and tautomeric equilibria between different tautomers were calculated using frequency calculations. Finally, this computational study reveals the thermal stability of the theoretical tautomers of mesoxaldehyde. We confirm our results through the synthesis of different heterocyclic compounds using mesoxaldehyde, which were identified using various spectral tools.

Conflicts of Interest

The authors declare no conflicts of interest regarding the publication of this paper.

References

[1] Kipnis, A.Y., Yavelov, B.E. and Rowlinson, J.S. (1996) Van der Waals and Molecular Science. Oxford University Press. https://doi.org/10.1093/oso/9780198552109.001.0001

[2] Katundu, S.M. (2017) Computational Studies of Lactam Tautomers by Using HF and DFT Methods in Gas and Solvent Phase. Master's Thesis, University of Dodoma.

[3] Szabo, A. and Ostlund, N.S. (1996) Modern Quantum Chemistry: Introduction to Advanced Electronic Structure Theory. Courier Corporation. https://scholar.google.com/scholar?cites=11787991376577675180&as_sdt=2005&sciodt=0,5&hl=en

[4] Hartree, D.R. (1928) The Wave Mechanics of an Atom with a Non-Coulomb Central Field. Part I. Theory and Methods. *Mathematical Proceedings of the Cambridge Philosophical Society*, **24**, 89-110. https://doi.org/10.1017/s0305004100011919

[5] Lee, C., Yang, W. and Parr, R.G. (1988) Development of the Colle-Salvetti Correlation-Energy Formula into a Functional of the Electron Density. *Physical Review B*, **37**, 785-789. https://doi.org/10.1103/physrevb.37.785

[6] Christopher, J.C. (2002) Essentials of Computational Chemistry. Wiley.

[7] Jensen, F. (2007) Introduction to Computational Chemistry. 2nd Edition, John Wiley & Sons Ltd.

[8] Hohenberg, P. and Kohn, W. (1964) Inhomogeneous Electron Gas. *Physical Review*, **136**, B864-B871. https://doi.org/10.1103/physrev.136.b864

[9] Kohn, W., Becke, A.D. and Parr, R.G. (1996) Density Functional Theory of Electronic Structure. *The Journal of Physical Chemistry*, **100**, 12974-12980. https://doi.org/10.1021/jp960669l

[10] Foresman, J.B. and Frisch, E. (1996) Exploring. Chemistry with Electronic Structure Methods. 2nd Edition, Gaussian, Inc.

[11] Becke, A.D. (1998) A New Inhomogeneity Parameter in Density-Functional Theory. *The Journal of Chemical Physics*, **109**, 2092-2098. https://doi.org/10.1063/1.476722

[12] Tozer, D.J. (1998) Effective Homogeneity of the Exchange-Correlation Energy Functional. *Physical Review A*, **58**, 3524-3527. https://doi.org/10.1103/physreva.58.3524

[13] Miehlich, B., Savin, A., Stoll, H. and Preuss, H. (1989) Results Obtained with the Correlation Energy Density Functionals of Becke and Lee, Yang and Parr. *Chemical Physics Letters*, **157**, 200-206. https://doi.org/10.1016/0009-2614(89)87234-3

[14] Senthilkumar, K. and Kolandaivel, P. (2002) Quantum Chemical Studies on Tautomerism of Barbituric Acid in Gas Phase and in Solution. *Journal of Computer-Aided Molecular Design*, **16**, 263-272. https://doi.org/10.1023/a:1020273219651

[15] Beytur, M. and Avinca, I. (2021) Molecular, Electronic, Nonlinear Optical and Spectroscopic Analysis of Heterocyclic 3-Substituted-4-(3-Methyl-2-Thienylmethyleneamino)-4,5-Dihydro-1*h*-1,2,4-Triazol-5-Ones: Experiment and DFT Calculations. *Heterocyclic Communications*, **27**, 1-16. https://doi.org/10.1515/hc-2020-0118

[16] March, T.J. (1992) Advanced Organic Chemistry. 4th Edition, Wiley, 330-335.

[17] El Kadem, H. and Abdel Rahman, M.M.A. (1966) Studies on the Products Obtained by the Periodate Oxidation of the Osazones. *Carbohydrate Research*, **3**, 25-31. https://doi.org/10.1016/S0008-6215(00)82292-2

[18] Vakili, M., Nekoei, A., Tayyari, S.F., Kanaani, A. and Sanati, N. (2012) Conformation, Molecular Structure, and Intramolecular Hydrogen Bonding of 1,1,1-Trifluoro-5,5-Dimethyl-2,4-Hexanedione. *Journal of Molecular Structure*, **1021**, 102-111. https://doi.org/10.1016/j.molstruc.2012.04.009

[19] Berenji, A.R., Tayyari, S.F., Rahimizadeh, M., Eshghi, H., Vakili, M. and Shiri, A. (2013) Structure and Vibrational Analysis of Methyl 3-Amino-2-Butenoate. *Spectrochimica Acta Part A*: *Molecular and Biomolecular Spectroscopy*, **102**, 350-357. https://doi.org/10.1016/j.saa.2012.10.042

[20] Gilli, G., Bellucci, F., Ferretti, V. and Bertolasi, V. (1989) Evidence for Resonance-Assisted Hydrogen Bonding from Crystal-Structure Correlations on the Enol Form of the .*β*.-Diketone Fragment. *Journal of the American Chemical Society*, **111**, 1023-1028. https://doi.org/10.1021/ja00185a035

[21] Gilli, G. and Gilli, P. (2009) The Nature of the Hydrogen Bond: Outline of a Comprehensive Hydrogen. Oxford University Press. https://doi.org/10.1093/acprof:oso/9780199558964.001.0001

[22] Caricato, M. and Frisch, M.J. (Eds.) (2009) Gaussian 09: IOps Reference. Gaussian.

[23] Møller, C. and Plesset, M.S. (1934) Note on an Approximation Treatment for Many-Electron Systems. *Physical Review*, **46**, 618-622. https://doi.org/10.1103/physrev.46.618

[24] Becke, A.D. and Roussel, M.R. (1989) Exchange Holes in Inhomogeneous Systems: A Coordinate-Space Model. *Physical Review A*, **39**, 3761-3767. https://doi.org/10.1103/physreva.39.3761

[25] Azeem, U., Khera, R.A., Naveed, A., Imran, M., Assiri, M.A., Khalid, M., *et al.* (2021) Tuning of a A-A-D-A-A-Type Small Molecule with Benzodithiophene as a Central Core with Efficient Photovoltaic Properties for Organic Solar Cells. *ACS Omega*, **6**, 28923-28935. https://doi.org/10.1021/acsomega.1c03975

[26] Khalid, M., Murtaza, S., Gull, K., Abid, S., Imran, M. and Braga, A.A.C. (2024) Influence of Acceptors on the Optical Nonlinearity of 5*h*-4-Oxa-1,6,9-Trithia-Cyclopenta[*b*]-As-Indacene-Based Chromophores with a Push-Pull Assembly: A DFT Approach. *RSC Advances*, **14**, 1169-1185. https://doi.org/10.1039/d3ra06673h

[27] Adeel, M., Khalid, M., Ullah, M.A., Muhammad, S., Khan, M.U., Tahir, M.N., *et al.* (2021) Exploration of CH···F & CF···H Mediated Supramolecular Arrangements into Fluorinated Terphenyls and Theoretical Prediction of Their Third-Order Nonlinear Optical Response. *RSC Advances*, **11**, 7766-7778. https://doi.org/10.1039/d0ra08528f

[28] Ayyash, A.N. (2022) Theoretical Study of Some Spectral Properties of Laser Dye by Using Gaussian Program and Gauss View Depending on Density Function Theory. https://ssrn.com/abstract=4277430

[29] Zhurko, G.A. and Zhurko, D.A. (2005) ChemCraft: Tool for Treatment of Chemical Data, Lite Version Build 08 (Freeware). https://www.chemcraftprog.com/download.html

[30] Politzer, P. and Murray, J.S. (1996) Relationships of Electrostatic Potentials to

Intrinsic Molecular Properties. In: *Theoretical and Computational Chemistry*, Elsevier, Vol. 3, 649-660. https://doi.org/10.1016/s1380-7323(96)80056-2

[31] Rocha, M., Di Santo, A., Ben Altabef, A. and M. Gil, D. (2019) Intermolecular Interactions, Spectroscopic and Theoretical Investigation of 4-aminoacetophenone. *International Journal of Advanced Chemistry*, **7**, 1-12. https://doi.org/10.14419/ijac.v7i1.14703

[32] Amalanathan, M., Rastogi, V.K., Hubert Joe, I., Palafox, M.A. and Tomar, R. (2011) Density Functional Theory Calculations and Vibrational Spectral Analysis of 3,5-(Dinitrobenzoic Acid). *Spectrochimica Acta Part A*: *Molecular and Biomolecular Spectroscopy*, **78**, 1437-1444. https://doi.org/10.1016/j.saa.2011.01.023

[33] Vivas-Reyes, R., Núñez-Zarur, F. and Martınez, E. (2008) Electronic Structure and Reactivity Analysis for a Set of Zn-Chelates with Substituted 8-Hydroxyquinoline Ligands and Their Application in OLED. *Organic Electronics*, **9**, 625-634. https://doi.org/10.1016/j.orgel.2008.04.004

[34] Karabacak, M. and Kurt, M. (2008) Comparison of Experimental and Density Functional Study on the Molecular Structure, Infrared and Raman Spectra and Vibrational Assignments of 6-Chloronicotinic Acid. *Spectrochimica Acta Part A*: *Molecular and Biomolecular Spectroscopy*, **71**, 876-883. https://doi.org/10.1016/j.saa.2008.02.014

[35] Tayyari, S.F., Zahedi-Tabrizi, M., Azizi-Toupkanloo, H., Hepperle, S.S. and Wang, Y.A. (2010) The Nature of Intramolecular Hydrogen Bond in 2-Nitromalonaldehyde. *Chemical Physics*, **368**, 62-65. https://doi.org/10.1016/j.chemphys.2009.12.016

[36] Belova, N.V., Oberhammer, H., Trang, N.H. and Girichev, G.V. (2014) Tautomeric Properties and Gas-Phase Structure of Acetylacetone. *The Journal of Organic Chemistry*, **79**, 5412-5419. https://doi.org/10.1021/jo402814c

[37] Kwiatkowski, J.S., Zielinski, T.J. and Rein, R. (1986) Quantum-Mechanical Prediction of Tautomeric Equilibria. *Advances in Quantum Chemistry*, **18**, 85-130. https://doi.org/10.1016/s0065-3276(08)60048-9

[38] Mulliken, R.S. (1955) Electronic Population Analysis on LCAO-MO Molecular Wave Functions. I. *The Journal of Chemical Physics*, **23**, 1833-1840. https://doi.org/10.1063/1.1740588

[39] Balachandran, V. and Parimala, K. (2012) Tautomeric Purine Forms of 2-Amino-6-Chloropurine (N9H10 and N7H10): Structures, Vibrational Assignments, NBO Analysis, Hyperpolarizability, HOMO-LUMO Study Using B3 Based Density Functional Calculations. *Spectrochimica Acta Part A*: *Molecular and Biomolecular Spectroscopy*, **96**, 340-351. https://doi.org/10.1016/j.saa.2012.05.050

[40] Lakshmi, A. and Balachandran, V. (2013) Rotational Isomers, NBO and Spectral Analyses of N-(2-Hydroxyethyl) Phthalimide Based on Quantum Chemical Calculations. *Journal of Molecular Structure*, **1033**, 40-50. https://doi.org/10.1016/j.molstruc.2012.08.002

[41] Ramalingam, S., Karabacak, M., Periandy, S., Puviarasan, N. and Tanuja, D. (2012) Spectroscopic (Infrared, Raman, UV and NMR) Analysis, Gaussian Hybrid Computational Investigation (MEP Maps/HOMO and LUMO) on Cyclohexanone Oxime. *Spectrochimica Acta Part A*: *Molecular and Biomolecular Spectroscopy*, **96**, 207-220. https://doi.org/10.1016/j.saa.2012.03.090

[42] Arshad, M.N., Mahmood, T., Khan, A.F., Zia-Ur-Rehman M., Asiri, A.M, Khan, I.U. and Nisa, R.U. (2015) Synthesis, Crystal Structure and Spectroscopic Properties of 1,2-Benzothiazine Derivatives: An Experimental and DFT Study. *Chinese Journal of Structural Chemistry*, **34**, 15-25. https://api.semanticscholar.org/CorpusID:101481196%7D

[43] Arshad, M.N., Asiri, A.M., Alamry, K.A., Mahmood, T., Gilani, M.A., Ayub, K., *et al.* (2015) Synthesis, Crystal Structure, Spectroscopic and Density Functional Theory (DFT) Study of N-[3-Anthracen-9-yl-1-(4-Bromo-Phenyl)-Allylidene]-n-Benzenesulfonohydrazine. *Spectrochimica Acta Part A*: *Molecular and Biomolecular Spectroscopy*, **142**, 364-374. https://doi.org/10.1016/j.saa.2015.01.101

[44] Fleming, I. and Wiley, J. (1976) Frontier Orbitals and Organic Chemical Reactions. Sons LTD, 879-880.

[45] Aihara, J. (1999) Reduced HOMO-LUMO Gap as an Index of Kinetic Stability for Polycyclic Aromatic Hydrocarbons. *The Journal of Physical Chemistry A*, **103**, 7487-7495. https://doi.org/10.1021/jp990092i

[46] Ruiz-Morales, Y. (2002) HOMO-LUMO Gap as an Index of Molecular Size and Structure for Polycyclic Aromatic Hydrocarbons (PAHs) and Asphaltenes: A Theoretical Study. I. *The Journal of Physical Chemistry A*, **106**, 11283-11308. https://doi.org/10.1021/jp021152e

[47] Padmaja, L., Ravikumar, C., Sajan, D., Hubert Joe, I., Jayakumar, V.S., Pettit, G.R., *et al.* (2008) Density Functional Study on the Structural Conformations and Intramolecular Charge Transfer from the Vibrational Spectra of the Anticancer Drug Combretastatin-A2. *Journal of Raman Spectroscopy*, **40**, 419-428. https://doi.org/10.1002/jrs.2145

[48] Ravikumar, C., Joe, I.H. and Jayakumar, V.S. (2008) Charge Transfer Interactions and Nonlinear Optical Properties of Push-Pull Chromophore Benzaldehyde Phenylhydrazone: A Vibrational Approach. *Chemical Physics Letters*, **460**, 552-558. https://doi.org/10.1016/j.cplett.2008.06.047

[49] Curtiss, L.A., Redfern, P.C., Raghavachari, K. and Pople, J.A. (1998) Assessment of Gaussian-2 and Density Functional Theories for the Computation of Ionization Potentials and Electron Affinities. *The Journal of Chemical Physics*, **109**, 42-55. https://doi.org/10.1063/1.476538

[50] Sheela, N.R., Muthu, S. and Sampathkrishnan, S. (2014) Molecular Orbital Studies (Hardness, Chemical Potential and Electrophilicity), Vibrational Investigation and Theoretical NBO Analysis of 4-4'-(1h-1,2,4-Triazol-1-Yl Methylene) Dibenzonitrile Based on Abinitio and DFT Methods. *Spectrochimica Acta Part A*: *Molecular and Biomolecular Spectroscopy*, **120**, 237-251. https://doi.org/10.1016/j.saa.2013.10.007

[51] Parr, R.G., Donnelly, R.A., Levy, M. and Palke, W.E. (1978) Electronegativity: The Density Functional Viewpoint. *The Journal of Chemical Physics*, **68**, 3801-3807. https://doi.org/10.1063/1.436185

[52] Parr, R.G. and Pearson, R.G. (1983) Absolute Hardness: Companion Parameter to Absolute Electronegativity. *Journal of the American Chemical Society*, **105**, 7512-7516. https://doi.org/10.1021/ja00364a005

[53] Parr, R. (1989) Density Functional Theory of Atoms and Molecules. Oxford University Press, 101.

[54] Parr, R.G., Szentpály, L.v. and Liu, S. (1999) Electrophilicity Index. *Journal of the American Chemical Society*, **121**, 1922-1924. https://doi.org/10.1021/ja983494x

[55] Domingo, L.R., Chamorro, E. and Pérez, P. (2008) Understanding the Reactivity of Captodative Ethylenes in Polar Cycloaddition Reactions. A Theoretical Study. *The Journal of Organic Chemistry*, **73**, 4615-4624. https://doi.org/10.1021/jo800572a

[56] Jaramillo, P., Domingo, L.R., Chamorro, E. and Pérez, P. (2008) A Further Exploration of a Nucleophilicity Index Based on the Gas-Phase Ionization Potentials. *Journal of Molecular Structure*: *Theochem*, **865**, 68-72. https://doi.org/10.1016/j.theochem.2008.06.022

[57] Deuri, S. and Phukan, P. (2012) A DFT Study on Nucleophilicity and Site Selectivity of Nitrogen Nucleophiles. *Computational and Theoretical Chemistry*, **980**, 49-55. https://doi.org/10.1016/j.comptc.2011.11.017

[58] Prabavathi, N. and Senthil Nayaki, N. (2014) The Spectroscopic (FT-IR, Ft-Raman and NMR), First Order Hyperpolarizability and HOMO-LUMO Analysis of 2-Mercapto-4(3h)-Quinazolinone. *Spectrochimica Acta Part A*: *Molecular and Biomolecular Spectroscopy*, **129**, 572-583. https://doi.org/10.1016/j.saa.2014.04.041

[59] Prasad, M.V.S., Chaitanya, K., UdayaSri, N. and Veeraiah, V. (2013) Experimental and Theoretical (HOMO, LUMO, NBO Analysis and NLO Properties) Study of 7-Hydroxy-4-Phenylcoumarin and 5,7-Dihydroxy-4-Phenylcoumarin. *Journal of Molecular Structure*, **1047**, 216-228. https://doi.org/10.1016/j.molstruc.2013.04.066

[60] Fatma, S., Bishnoi, A. and Verma, A.K. (2015) Synthesis, Spectral Analysis (FT-IR, 1H NMR, 13C NMR and UV-Visible) and Quantum Chemical Studies on Molecular Geometry, NBO, NLO, Chemical Reactivity and Thermodynamic Properties of Novel 2-Amino-4-(4-(Dimethylamino)Phenyl)-5-Oxo-6-Phenyl-5,6-Dihydro-4h-pyrano[3,2-c]Quinoline-3-Carbonitrile. *Journal of Molecular Structure*, **1095**, 112-124. https://doi.org/10.1016/j.molstruc.2015.04.026

[61] Vitnik, V.D., Vitnik, Ž.J., Banjac, N.R., Valentić, N.V., Uščumlić, G.S. and Juranić, I.O. (2014) Quantum Mechanical and Spectroscopic (FT-IR, 13C, 1H NMR and UV) Investigations of Potent Antiepileptic Drug 1-(4-Chloro-Phenyl)-3-Phenyl-Succinimide. *Spectrochimica Acta Part A*: *Molecular and Biomolecular Spectroscopy*, **117**, 42-53. https://doi.org/10.1016/j.saa.2013.07.099

[62] Çatıkkaş, B., Aktan, E. and Seferoğlu, Z. (2012) DFT, Ft-Raman, FTIR, NMR, and UV-Vis Studies of a Hetarylazo Indole Dye. *International Journal of Quantum Chemistry*, **113**, 683-689. https://doi.org/10.1002/qua.24043